

B 4 Brownian Dynamics simulations

G. Nägele

Institut für Festkörperforschung

Forschungszentrum Jülich GmbH

Contents

1	Introduction	2
2	Single-particle Langevin equations and time scales	3
2.1	Velocity Langevin equation	3
2.2	Positional Langevin equation	5
3	Positional Langevin equations for interacting particles	8
3.1	Brownian Dynamics finite difference scheme	8
3.2	Equivalence with many-particle diffusion equation	10
3.3	Simulation details	13
3.4	Simulation of particles with hard-body interaction	17
4	Brownian Dynamics simulations with hydrodynamic interactions	21
4.1	Hydrodynamic interactions of spheres	22
4.2	Generalized Smoluchowski equation with HI	24
4.3	Finite difference algorithms including HI	26
5	Summary and Outlook	30

1 Introduction

Mesoscopically large particles (e.g., colloidal particles, proteins or polymers) suspended in a low-molecular-weight fluid like water experience many random kicks from the fluid molecules. When observed with a coarse-grained time resolution where the fast motion of the fluid molecules is not resolved, these random kicks result in an erratic Brownian motion of the mesoparticles. Due to the many collisions with the fluid molecules, and the strong fluid friction experienced through the large surface, the distribution of momenta of the particles reaches Maxwellian equilibrium long before their positions have changed appreciably. In fact, when studying physical phenomena like particle diffusion, suspension rheology and microstructural behavior one is concerned only with the slow time evolution of the particle configuration.

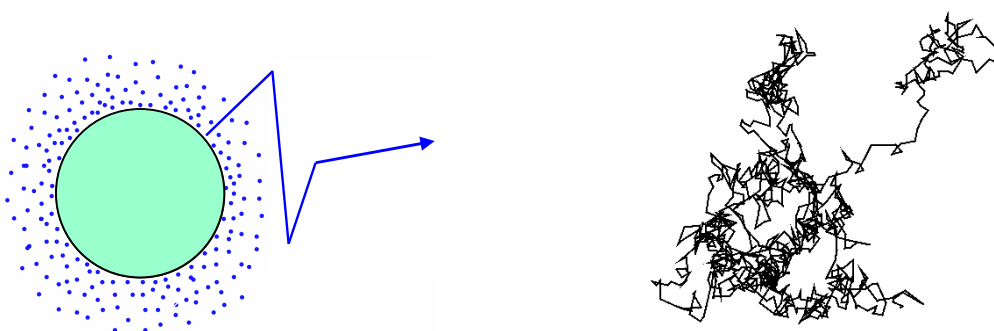


Fig. 1: *Left: colloidal sphere bombarded by fast solvent molecules. Right: random walk trajectory of a colloidal particle.*

The Brownian Dynamics (BD) simulation technique is a mesoscale method which takes advantage of the fact that there is a large separation of time scales between the rapid momentum relaxation and the much slower positional changes of the Brownian particles. At the core of this technique is a coupled set of many-particle Langevin equations describing the evolution of the particle positions, with the momenta integrated out of the description. In these stochastic differential equations, the influence of the collisions by solvent molecules is represented on a coarse-grained level by stochastic forces or velocities and by hydrodynamic drag forces. In addition, the particles are subject to solvent-averaged direct interaction forces. The Langevin equations are solved numerically by a forward integration scheme with discrete time-steps to generate representative particle trajectories. In this scheme the stochastic forces are simulated by random numbers. Thus, in BD simulations, an ensemble of stochastic trajectories is generated. By averaging over trajectories created after an equilibration run, one can calculate equilibrium statistical averages like radial distribution functions, as well as general time correlation functions, for example mean-square displacements, van Hove functions, and dynamic viscosities. Accordingly, the BD simulation method can be considered to be between the Monte Carlo and Molecular Dynamics methods, sharing the element of randomness with the first, and the continuity (albeit with strong irregularity) of trajectories in configuration space with the latter.

In the Brownian Dynamics methodology the fluid is described macroscopically as a continuum which, on the coarse-grained level where configurational changes take place, obeys the linearized and stationary Navier-Stokes equation. This equation is commonly referred to as the creeping flow or Stokes equation, and it describes incompressible lamellar flow at low Reynold's

numbers. The penalty incurred for treating the solvent macroscopically is that, in addition to the direct inter-particle forces, one needs to account for the so-called hydrodynamic interactions (HI) acting between Brownian particles. This long-range type of dynamic interaction is transmitted by complicated fluid flow patterns created by the moving particles. In concentrated dispersions, HI cause a non-pairwise additive coupling of the particle drift velocities as well as a coupling of the Brownian stochastic forces appearing in the Langevin equations. This coupling gives rise to significant computational difficulties in the case of BD simulations where HI are included.

In this lecture, I will first explain the essentials of the BD simulation technique in the so-called free-draining approximation where HI are totally ignored (section 3). The complications arising from the inclusion of HI will be discussed in section 4 on various levels of approximation. A few applications will be discussed for systems without HI and with HI effects included. Section 5 contains a summary, and a short overview on recent developments in the field of Brownian Dynamics.

2 Single-particle Langevin equations and time scales

We start our discussion of Brownian Dynamics simulations by considering the most simple case of a single mesoscale particle immersed in a fluid of small molecules. The motion of this particle will be explored on two levels of description, firstly on a time scale where its inertia is resolved, and secondly on a coarser scale where its diffusive random excursions become apparent. The present section introduces salient concepts like Langevin equations and time scale separation. These concepts are needed in sections 3 and 4 where dispersions of interacting particles are discussed.

2.1 Velocity Langevin equation

Consider a spherical particle of mass m and radius $5 \text{ nm} < a < 1 \text{ }\mu\text{m}$, suspended in an unbound and quiescent solvent of much smaller molecules with a linear size of a few Ångströms. Such a large colloidal particle is subject to incessant collisions with the solvent molecules, each collision lasting of the order of τ_s (with $\tau_s \sim 10^{-13} \text{ s}$ for water). Whereas the momentum of the particle is scarcely changed during a single collision, the particle executes a slow erratic motion when observed on a coarse-grained time scale much larger than τ_s (cf. Fig. 1).

Let $\mathbf{r}(t)$ be the position vector of the particle at time t . For a time resolution of $\Delta t \gg \tau_s$, the equation of motion for the translational velocity $\mathbf{v}(t) = \dot{\mathbf{r}}(t)$ is given by the single-particle Langevin equation [1]

$$m\ddot{\mathbf{r}}(t) = -\zeta_0\dot{\mathbf{r}}(t) + \mathbf{F}^s(t). \quad (1)$$

The sphere experiences through the solvent molecules impacts an average friction force $-\zeta_0\dot{\mathbf{r}}$, and a fluctuating stochastic force $\mathbf{F}^s(t)$. On the coarse-grained level where Eq. (1) applies, the solvent behaves like a continuum. Consequently the friction coefficient, ζ_0 , of a sphere can be approximated by its Stokes value, $\zeta_0 = 6\pi\eta_0 a$, where η_0 is the shear viscosity of the suspending fluid. The random force describes the accumulative effect of many solvent molecules' collisions which are statistically independent for times large compared to τ_s . According to the central limit theorem of probability theory, a sum of many independent random variables with

finite second moments of their probability distributions converges towards a Gaussian random variable (see [2] for a more precise statement of this theorem). Therefore, we can describe $\mathbf{F}^s(t)$ as a Gaussian-distributed fluctuating quantity whose statistical properties are completely determined by its first moment and its covariance matrix. Specifically

$$\langle \mathbf{F}^s(t) \rangle = 0, \quad (2)$$

and the covariance matrix is given in polyadic tensor notation by

$$\langle \mathbf{F}^s(t) \mathbf{F}^s(t') \rangle = \mathbf{1} \Gamma \delta(t - t'). \quad (3)$$

Here, $\langle \dots \rangle$ is an average over the solvent collisions, Γ measures the strength of the fluctuating force, and $\mathbf{1}$ is the 3×3 unit matrix expressing spatial isotropy and the fact that the three Cartesian components $F_\alpha^s(t)$, with $\alpha \in \{x, y, z\}$, are mutually uncorrelated. The delta function indicates that the random forces are uncorrelated on the time scale of the particle motion, i.e., the forces are an example of Gaussian white noise. According to Wick's theorem for Gaussian random variables (see [2]), all multi-time correlation functions of a force component $F = F_\alpha^s$ with even time points can be pairwise factorized as ($n = 2, 3, \dots$)

$$\begin{aligned} \langle F(t_1) \cdots F(t_{2n}) \rangle &= \sum_P \langle F(t_{i_1}) F(t_{i_2}) \rangle \cdots \langle F(t_{i_{2n-1}}) F(t_{i_{2n}}) \rangle \\ &= \Gamma^n \sum_P \delta(t_{i_1} - t_{i_2}) \cdots \delta(t_{i_{2n-1}} - t_{i_{2n}}). \end{aligned} \quad (4)$$

The sum extends over those out of the $(2n)!/(2^n n!)$ pairwise factorizations P of $\{1, \dots, 2n\}$ that lead to different expressions. All correlations functions with odd time-points are zero.

The random force in the Langevin equation is described as a time-dependent random variable (i.e. a stochastic process) defined only by its statistical properties. These statistical properties relate to an ensemble of independent Brownian particles each of which is a realization of a diffusion process. The statistical averages $\langle \dots \rangle$ are interpreted here as averages over this ensemble of systems. Time integration of Eq. (1) for a given realization of $\mathbf{F}^s(t)$ leads to

$$\mathbf{v}(t) = \mathbf{v}_0 e^{-t/\tau_B} + \frac{1}{m} \int_0^t du e^{-(t-u)/\tau_B} \mathbf{F}^s(u) \quad (5)$$

where \mathbf{v}_0 is the initial velocity. Averaging over a sub-ensemble of particles with equal initial velocities gives

$$\langle \mathbf{v}(t) \rangle = \mathbf{v}_0 e^{-t/\tau_B}, \quad (6)$$

for the mean velocity which decays towards zero as quantified by the characteristic momentum relaxation time $\tau_B = m/\zeta_0$. Using typical values for aqueous suspensions of colloidal spheres, e.g., $a = 100$ nm, particle mass density $\rho_p = 1$ kg/m³, and shear viscosity of water with $\eta_0 = 0.01$ poise, one obtains $\tau_B \approx 2.2 \times 10^{-9}$ s, showing that $\tau_B \gg \tau_s$ (cf. Fig. 2).

We can next determine the mean of the squared velocity using the delta correlation in Eq. (3),

$$\langle \mathbf{v}(t)^2 \rangle = \mathbf{v}_0^2 e^{-2t/\tau_B} + \frac{3\Gamma}{2m\zeta_0} (1 - e^{-2t/\tau_B}). \quad (7)$$

Equipartition of the kinetic energy in equilibrium demands, for $t \rightarrow \infty$, that $\mathbf{v}^2(\infty) = 3k_B T/m$ which serves to determine Γ as

$$\Gamma = 2k_B T \zeta_0. \quad (8)$$

This relation comprises a fluctuation-dissipation theorem relating the strength of the fluctuating force to the mean particle friction coefficient (and temperature T), thereby reflecting their common origin in the interaction between the mesoparticle and the solvent molecules.

So far we have considered the Brownian motion of a particle with given fixed initial velocity \mathbf{v}_0 . To describe a system in equilibrium we need to average over a Maxwellian distribution of initial velocities. Multiplication of Eq. (6) by \mathbf{v}_0 and subsequent averaging over solvent collisions *and* initial velocities gives

$$\phi_v(t) \equiv \frac{1}{d} \langle \mathbf{v}(t) \cdot \mathbf{v}(0) \rangle_{eq} = \frac{k_B T}{m} \exp \{-t/\tau_B\} \quad (9)$$

for the velocity auto-correlation function, $\phi_v(t)$, of an isolated Brownian sphere in $d = 3$ spatial dimensions. According to Eq. (9), momenta lose their memory within a time interval of the order of τ_B . Next, using that $\mathbf{r}(t) - \mathbf{r}_0 = \int_0^t du \mathbf{v}(u)$, one can easily show for a system in a stationary state that $\phi_v(t)$ is related to the mean-square displacement (MSD) of a particle, $W(t)$, by

$$W(t) \equiv \frac{1}{2d} \langle [\mathbf{r}(t) - \mathbf{r}(0)]^2 \rangle_{eq} = \int_0^t du (t-u) \phi_v(u). \quad (10)$$

For convenience, we have absorbed the factor $1/(2d)$ into the definition of $W(t)$. Relation (10) is valid also for non-dilute systems of interacting particles. The MSD of an isolated sphere follows from substituting Eq. (9) into Eq. (10) as

$$W(t) = D_0 t \left[1 - \frac{\tau_B}{t} (1 - e^{-t/\tau_B}) \right] \rightarrow \begin{cases} \frac{k_B T}{2m} t^2, & \tau_s \ll t \ll \tau_B, \\ D_0 t, & t \gg \tau_B, \end{cases} \quad (11)$$

where the single-particle diffusion coefficient D_0 is related to the friction coefficient by the Stokes-Einstein-(Sutherland) relation

$$D_0 = \frac{k_B T}{\zeta_0}. \quad (12)$$

Equation (11) interpolates between ballistic flight behavior with Maxwell-distributed initial velocities for $t \ll \tau_B$, and linear diffusive behavior for $t \gg \tau_B$. Using once more the particle radius of $a = 100$ nm, we find $D_0 = 2.2 \times 10^{-12}$ m²/s for the diffusion coefficient.

2.2 Positional Langevin equation

As was seen, the MSD of an *isolated* particle grows linearly according to $W(t) \approx D_0 t$ for *all* times $t \gg \tau_B$, i.e. for a coarse time resolution where the momentum relaxation is not resolved. Consider for the time being a non-dilute suspension of interacting colloidal particles. To observe an appreciable change of configuration, a particle should have diffused a distance at least comparable to its own size. A characteristic time needed for a significant change in configuration is thus given by the structural relaxation time

$$\tau_a = a^2/D_0, \quad (13)$$

with $\tau_a = 4.7 \times 10^{-3}$ s for $a = 100$ nm, and $\tau_a = 4.7$ s for $a = 1$ micron. The crucial message to note is that $\tau_a \gg \tau_B$, i.e. there is a separation of time scales: The momentum of a colloidal

particle has relaxed long before any appreciable change in particle configuration is observed. A time resolution $\Delta t \gg \tau_B$ corresponds to a spatial resolution of $\Delta x \gg l_B \equiv \sqrt{D_0 \tau_B}$. A typical value is $l_B \approx 10^{-3}a$, and this illustrates additionally that the particle has hardly moved during τ_B .

The configurational evolution of mesoparticles observed with a time resolution $\Delta t \gg \tau_B$ on which the momenta are relaxed to Maxwellian equilibrium is commonly referred to as Brownian Dynamics, or likewise, as diffusive or Smoluchowski dynamics. Experimentally, diffusion of colloidal particles on the BD time scale can be probed conveniently using a variety of dynamic light scattering techniques [3].

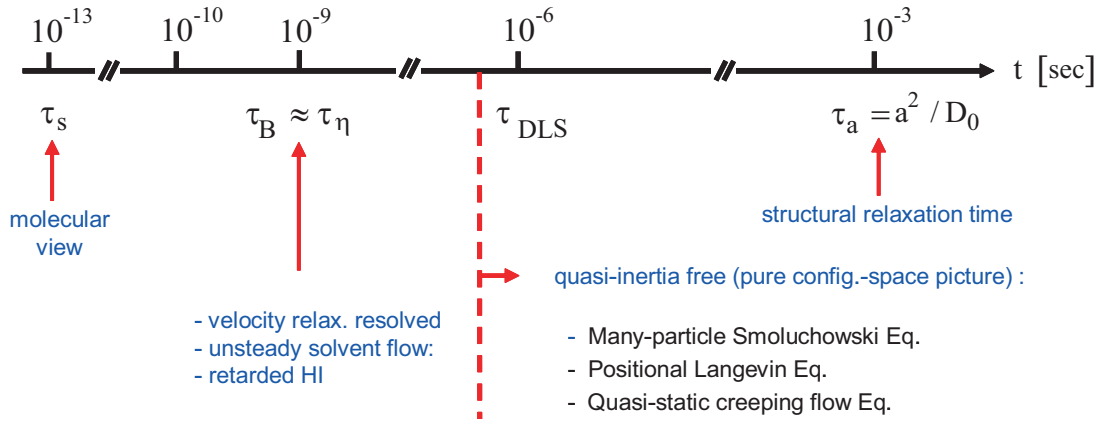


Fig. 2: Colloidal time scales: values are typical of colloidal spheres with radius $a = 100$ nm suspended in water. The time resolution of dynamic light scattering is characterized by τ_{DLS} .

On the BD time and length scales, changes in the particle velocity, which take place during $t \sim \tau_B$, are not resolved. Therefore, we may neglect the inertia-term $m\dot{\mathbf{v}}(t)$ in Eq. (1) as compared to the friction term. To see this explicitly, we estimate

$$m|\dot{\mathbf{v}}(t)| \sim m \frac{(k_B T/m)^{1/2}}{\Delta t} \ll \frac{(mk_B T)^{1/2}}{\tau_B} = \zeta_0 \left(\frac{k_B T}{m} \right)^{1/2} \sim \zeta_0 |\mathbf{v}(t)|. \quad (14)$$

Therefore, we obtain the *positional* Langevin equation for the Brownian Dynamics of an isolated particle,

$$\dot{\mathbf{r}}(t) = \frac{1}{\zeta_0} \mathbf{F}^s(t) \equiv \mathbf{v}^B(t), \quad (15)$$

valid for $\Delta t \gg \tau_B$ and $\Delta x \gg l_B$. This evolution equation for the particle position expresses a force-balance and implies quasi-inertia-free colloid motion for $t \gg \tau_B$. According to Eqs. (2)-(4), (8) and (12), $\mathbf{v}^B(t)$ is a Gaussian-distributed and δ -correlated random velocity, denoted as the Brownian velocity. It is fully characterized by the first two moments

$$\langle \mathbf{v}^B(t) \rangle = 0, \quad \langle \mathbf{v}^B(t) \mathbf{v}^B(t') \rangle = 2D_0 \mathbf{1} \delta(t - t'). \quad (16)$$

From integrating Eq. (15) over a time interval Δt , we get the finite-difference equation

$$\mathbf{r}(t_0 + \Delta t) - \mathbf{r}_0 = \int_{t_0}^{t_0 + \Delta t} du \mathbf{v}^B(u) = \sqrt{2D_0 \Delta t} \mathbf{n}, \quad (17)$$

where \mathbf{n} is a vector of mutually statistically independent Gaussian random *numbers* $\{n_\alpha\}$ of zero mean and variance 1. Explicitly

$$\langle \mathbf{n} \rangle = 0, \quad \langle \mathbf{n} \mathbf{n} \rangle = \mathbf{1}. \quad (18)$$

and higher-order moments $\langle n_\alpha^{2m-1} \rangle = 0$ and $\langle n_\alpha^{2m} \rangle = (2m-1)!!$ with $m \in \{2, 3, \dots\}$.

Note from Eq. (17) that the random displacement during τ is of $O(\tau^{1/2})$ only. On dividing Eq. (17) by Δt and trying to take the limit $\Delta t \rightarrow 0$, it becomes clear that the Brownian velocity does not exist in the sense of ordinary calculus. Strictly speaking, the stochastic trajectories generated by the positional Langevin equation are only continuous, but not differentiable. A mathematically sound interpretation of a Langevin equation with white noise like Eq. (15) can be given using the concept of a Wiener measure [2] related to the time integral over $\mathbf{v}^B(u)/D_0^{1/2}$. However, it suffices here to *interpret* the Langevin equation in terms of its finite difference form in Eq. (17). From the finite difference equation we infer that $\Delta \mathbf{r}^B(t) \equiv \mathbf{r}(t_0 + t) - \mathbf{r}(t_0)$ is a Gaussian random process with vanishing odd moments, and even moments determined as

$$\left\langle (\Delta \mathbf{r}^B(t))^2 \right\rangle_0 = 6D_0t, \quad \left\langle (\Delta \mathbf{r}^B(t))^{2n} \right\rangle_0 = O(t^n). \quad (19)$$

The conditional averages are performed over a sub-ensemble of particles of equal initial position \mathbf{r}_0 . The probability density function (pdf), $P(\Delta \mathbf{r}^B, t)$, for a displacement $\Delta \mathbf{r}^B$ during time t is thus

$$P(\Delta \mathbf{r}^B, t) = \{4\pi D_0t\}^{-3/2} \exp\left\{-\frac{(\Delta \mathbf{r}^B)^2}{4D_0t}\right\}. \quad (20)$$

This conditional pdf is the solution of the single-particle diffusion equation (Smoluchowski equation)

$$\frac{\partial}{\partial t} P(\Delta \mathbf{r}, t) = D_0 \nabla^2 P(\Delta \mathbf{r}, t), \quad (21)$$

subject to the initial condition $P(\Delta \mathbf{r}, t=0) = \delta(\Delta \mathbf{r})$. The single-particle diffusion equation is equivalent to the positional Langevin equation in a statistical sense: The former is a stochastic differential equation for an ensemble of particle trajectories whereas the latter determines the corresponding distribution function.

Before closing this section, I should point out that the velocity Langevin Eq. (1) does not apply to colloidal particles for $t \sim \tau_B$. In fact, it is valid only for times $t \gg \tau_\eta$ where solvent inertia is negligible [4, 5]. Here, $\tau_\eta = a^2 \rho_s / \eta_0 = (9/2)(\rho_s / \rho_p) \tau_B$ characterizes the time scale where solvent inertia matters. It is the time needed for a viscous shear wave, generated in the solvent by a sudden acceleration of the particle, to diffuse away across a distance a . The solvent mass density, ρ_s , is close to the particle mass density ρ_p . Otherwise the particle would fall out. Therefore τ_η and τ_B are of the same order of magnitude. For $t \sim \tau_B \approx \tau_\eta$, the fluid can not instantaneously follow changes in the particle velocity. This leads to an enlarged persistence in the velocity autocorrelations, not adequately described by δ -correlated random forces. The memory in the particle velocities can be accounted for by means of a generalized velocity Langevin equation with non-white (i.e., colored) random forces. Calculations based on this equation have revealed, in contrast to Eq. (11), that the MSD approaches its limiting form $W(t) \approx D_0t$ algebraically slowly rather than exponentially fast, i.e.

$$W(t) \approx D_0t \left[1 - \frac{2}{\sqrt{\pi}} \left(\frac{\tau_\eta}{t} \right)^{1/2} \right], \quad (22)$$

for $t \gg \tau_\eta$. Such an algebraic long-time tail in $W(t)$ has been observed in dynamic light scattering experiments on colloids [6]. Although Eq. (1) does not describe dilute colloidal dispersions for times $t \approx \tau_B$, it can be applied instead to aerosols like smoke particles in air, since in these systems one finds $\rho_s \ll \rho_p$ so that $\tau_\eta \ll \tau_B$.

Brownian Dynamics as described by positional Langevin equations is not plagued by solvent-inertia, since it addresses positional changes for times $t \gg \tau_B$ and distances $\Delta x \gg l_B$. On the BD time scale the particles *and* the solvent move quasi-inertia-free, and this gives rise to a pure configuration-space description. Fig. 2 provides a pictorial view of all colloidal time scales discussed in this section.

3 Positional Langevin equations for interacting particles

In this section, I will explain the Brownian Dynamics simulation technique for interacting mesoparticles in the *free-draining approximation*. In this approximation, only direct pair interactions are considered, such as excluded volume, van der Waals and electrostatic forces, to name a few possibilities. Solvent-mediated HI forces are neglected. This amounts to assuming that each particle experiences a background fluid unperturbed by the presence of the other particles. Thus, the net mean effect of the fluid is simply to exert a friction force on each particle independent of the location and velocity of the others. In real systems, the influence of HI on the dynamics is negligible only at strong dilution. Nonetheless, there are cases where dynamic properties of interest are largely determined by direct interactions. In addition, free-draining BD simulations are needed to quantify the importance of HI through comparison with computationally more expensive BD calculations where HI are considered. Free-draining simulations are also used to calculate static equilibrium properties, as these are independent of HI (cf. the discussion below).

3.1 Brownian Dynamics finite difference scheme

So far we have considered very dilute suspensions in which the individual particles could be considered as independent from each other. For non-dilute systems, interactions have to be taken into account. For simplicity, we consider a suspension of N identical spherical particles whose momentary centers are located at the points $\mathbf{X} = (\mathbf{r}_1, \dots, \mathbf{r}_N)^T$ as described by the $3N$ -dimensional column vector \mathbf{X} . The superscript denotes the operation of transposition. The particles are supposed to interact in a pairwise-additive way by an isotropic and solvent-averaged pair potential $u(r)$. We assume that $u(r)$ is soft without jumps or singularities (Lennard-Jones-type potentials for example). Particles with a genuine hard-body potential part, and a non-zero likelihood for configurations with particles in contact, require a special treatment in BD simulations. The discussion of hard-sphere-like systems will be postponed to subsection 3.4. For the N -body potential energy function, we may write

$$\Phi(\mathbf{X}) = \sum_{i < j} u(r_{ij}), \quad (23)$$

with continuous deterministic forces $\mathbf{F}_i(\mathbf{X}) = -\nabla_i \Phi(\mathbf{X})$ acting on particles $i \in \{1, \dots, N\}$. In addition, we require that $\Phi(\mathbf{X})$ is essentially constant across a distance l_B where a particle

relaxes its momentum, so that $l_B |\nabla_i \Phi(\mathbf{X})| \ll |\Phi(\mathbf{X})|$. The solvent far away from the particles is supposed to be at rest (quiescent suspension).

The positional Langevin equations for N interacting particles with HI disregarded is obtained as a straightforward generalization of Eq. (15), namely

$$\dot{\mathbf{r}}_i(t) = \mathbf{v}_i^D(\mathbf{X}(t)) + \mathbf{v}_i^B(t), \quad (24)$$

for $i = 1, \dots, N$, with the slowly varying deterministic drift velocities

$$\mathbf{v}_i^D(\mathbf{X}) = \beta D_0 \mathbf{F}_i(\mathbf{X}), \quad (25)$$

where $\beta = 1/(k_B T)$, and the rapidly fluctuating Brownian velocity parts $\mathbf{v}_i^B(t)$. Without Brownian random velocities, Eq. (24) describes the overdamped motion of particles subject to deterministic forces. These forces alone would relax the particle coordinates towards a configuration $\mathbf{X}^{(m)}$ where $\Phi(\mathbf{X})$ attains a minimum. The Brownian velocities mimic the effect of solvent collisions on the BD time scale. They prevent the particles from remaining at the minimum configuration $\mathbf{X}^{(m)}$, so that the configurational distribution at large times becomes an equilibrium one. This important point will be explained in more detail in subsection 3.2. As in the single-particle case, each $\mathbf{v}_i^B(t)$ is a Gaussian and white random variable, characterized by

$$\langle \mathbf{v}_i^B(t) \rangle = 0, \quad \langle \mathbf{v}_i^B(t) \mathbf{v}_j^B(t') \rangle = 2 D_0 \mathbf{1} \delta_{ij} \delta(t - t'). \quad (26)$$

The Brownian velocities of different particles are statistically independent since hydrodynamic coupling is disregarded. For an equilibrated system, we may interpret $\langle \dots \rangle$ as an average over $M \gg 1$ microscopically identical copies of the system, or as an average over a single system by following its N -particle trajectory with M measurements taken at widely separated time intervals.

The positional Langevin Eqs. (24) can be derived starting from the momentum Langevin equations in the free-draining approximation, viz. [5, 7]

$$m \ddot{\mathbf{r}}_i(t) = -\zeta_0 \dot{\mathbf{r}}_i(t) + \mathbf{F}_i(\mathbf{X}(t)) + \mathbf{F}_i^s(t). \quad (27)$$

This set of coupled equations is an extension of Eq. (1) to non-hydrodynamically interacting particles. The stochastic forces, $\mathbf{F}_i^s(t)$, are Gaussian distributed and δ -correlated in time, of mean zero and with the covariance matrix given by

$$\langle \mathbf{F}_i^s(t) \mathbf{F}_j^s(t') \rangle = 2 k_B T \zeta_0 \delta_{ij} \mathbf{1} \delta(t - t'). \quad (28)$$

In principle, the momentum Langevin equations should be applicable down to times $t \sim \tau_B$. In its present form, however, it neither accounts for the non-instantaneous response of the solvent to changes in the particle velocity, nor for the non-instantaneous (at times $t \sim \tau_\eta$) hydrodynamic interactions present in real suspensions. The positional Langevin equations follow from averaging Eq. (27) over a time-step $\tau_B \ll \Delta t \ll \tau_a$, using Eq. (14). This time-averaging amounts to the neglect of the particle acceleration term in the coarse-grained momentum Langevin equations, giving rise to the positional Langevin equations, with the Brownian velocities identified, using Eq. (12), as $\mathbf{v}_i^B(t) = \beta D_0 \mathbf{F}_i^s(t)$.

To obtain the finite-difference form of Eq. (24), we integrate over a small time-step $(t_0, t_0 + \tau)$, during which the initial configuration $\mathbf{X}_0 = \mathbf{X}(t_0)$ remains practically unchanged. This leads to

$$\mathbf{r}_i(t_0 + \tau) = \mathbf{r}_i(t_0) + \mathbf{v}_i^D(\mathbf{X}_0)\tau + \sqrt{2D_0\tau} \mathbf{n} + o(\tau), \quad (29)$$

with an error of order $o(\tau)$ made in using a finite time-step¹. Eq. (29) is a straightforward generalization of Eq. (17) to interacting particles. It is a stochastic first-order forward integration scheme, commonly referred to as *Ermak's scheme* [8], for the simultaneous displacement,

$$\Delta\mathbf{X}(\tau) \equiv \mathbf{X}(t_0 + \tau) - \mathbf{X}(t_0). \quad (30)$$

of N particles during a small time-step τ . All forces are calculated in the configuration at the beginning of the time-step. The Gaussian random vector \mathbf{n} has been introduced already in Eq. (18): at each time-step, the components n_α of \mathbf{n} are generated independently from a Gaussian distribution of zero mean and variance one. As in the single-particle case, we may interpret the positional Langevin equations in terms of its finite-difference form, to avoid mathematical difficulties with the δ -correlated noise.

The $3N$ -variable stochastic process $\mathbf{X}(t)$ is a so-called Markov process whose future is entirely determined by its presence. This can be seen from Eq. (29). The Markovian property is a consequence of dealing with a noise of zero correlation time, and with Langevin equations of first order in the time derivative. Eq. (29) implies further that $\mathbf{X}(\tau) \rightarrow \mathbf{X}_0$ for $\tau \rightarrow 0$, i.e. $\mathbf{X}(t)$ is a continuous process. However, due to the white noise contribution, the particle trajectories are nowhere differentiable (with probability one). The continuity of $\mathbf{X}(t)$ is expressed in the moments derived from the finite-difference equation. From averaging over a sub-ensemble of systems with equal initial configuration \mathbf{X}_0 , we obtain readily

$$\langle \Delta\mathbf{X}(\tau) \rangle_0 = \mathbf{v}^D(\mathbf{X}_0)\tau + o(\tau) \quad (31)$$

$$\langle \Delta\mathbf{X}(\tau) \Delta\mathbf{X}(\tau) \rangle_0 = 2D_0\tau \mathbf{1} + o(\tau) \quad (32)$$

$$\langle \Delta\mathbf{X}(\tau) \dots \Delta\mathbf{X}(\tau) \rangle_0 = o(\tau), \quad (33)$$

where all higher-order polyadic products involving more than two $\Delta\mathbf{X}(\tau)$ are small of order $o(\tau)$. A small time-step implies a small configurational change for the large and heavy Brownian particles. In Eq. (32), $\mathbf{1}$ denotes the $3N \times 3N$ unit matrix, and $\mathbf{v}^D = (\mathbf{v}_1^D, \dots, \mathbf{v}_N^D)^T$ is the $3N$ -dimensional column vector of drift velocities.

3.2 Equivalence with many-particle diffusion equation

To gain information on the long-time behavior of the N -particle system described by the positional Langevin equations, we will explore the behavior of the pdf $P(\mathbf{X}, t)$ for finding the system in configuration \mathbf{X} at time t . Our major task will be to derive an evolution equation for the pdf.

From the moment relations (31-33) and the finite-difference equation, we note that during the time-step $\tau_B \ll \tau \ll \tau_a$, each particle i diffuses independently from the others in a constant force field, $\mathbf{F}_i(\mathbf{X}_0)$, determined by the configuration at the beginning of the time-step. Hence the

¹ A is of order $o(\tau)$ if $\lim_{\tau \rightarrow 0} A/\tau = 0$; likewise $A = O(\tau)$ when $\lim_{\tau \rightarrow 0} A/\tau$ is finite and non-zero.

short-time conditional pdf, $W_c(\mathbf{X}, \tau | \mathbf{X}_0)$, for a configurational displacement $\mathbf{X}_0 \rightarrow \mathbf{X}$ during τ , factorizes in a product of single-particle Gaussian distribution functions with non-zero drift velocities,

$$\begin{aligned} W_c(\mathbf{X}, \tau | \mathbf{X}_0) &= \{4\pi D_0 \tau\}^{-3N/2} \exp\left\{-\frac{1}{4D_0 \tau} [\mathbf{X} - \mathbf{X}_0 - \tau \mathbf{v}^D(\mathbf{X}_0)]^2\right\} \\ &= \prod_{i=1}^N \{4\pi D_0 \tau\}^{-3/2} \exp\left\{-\frac{1}{4D_0 \tau} [\mathbf{r}_i - \mathbf{r}_{i0} - \tau \mathbf{v}_i^D(\mathbf{X}_0)]^2\right\}. \end{aligned} \quad (34)$$

Differentiation of this expression with respect to time shows that W_c solves the diffusion equation,

$$\frac{\partial}{\partial \tau} W_c(\mathbf{X}, \tau | \mathbf{X}_0) = -\mathbf{v}^D(\mathbf{X}_0) \cdot \nabla W_c(\mathbf{X}, \tau | \mathbf{X}_0) + D_0 \nabla^2 W_c(\mathbf{X}, \tau | \mathbf{X}_0), \quad (35)$$

subject to the initial condition $W_c(\mathbf{X}, 0 | \mathbf{X}_0) = \delta(\mathbf{X} - \mathbf{X}_0) = \prod_i \delta(\mathbf{r}_i - \mathbf{r}_{i0})$. We have introduced here the $3N$ -dimensional nabla operator $\nabla = (\nabla_1, \dots, \nabla_N)$.

In general, $\mathbf{X}(t)$ is a Gaussian process only for times $\tau \ll \tau_a$. It inherits the Gaussian property from the Brownian velocities provided the positional Langevin equations express a linear relationship. For non-linear drift velocities, $\mathbf{X}(t)$ is non-Gaussian distributed for times $t \sim \tau_a$. Then we must distinguish the exact transition pdf $P_c(\mathbf{X}, t | \mathbf{X}_0)$ from its short-time approximation W_c . To determine $P_c(\mathbf{X}, t | \mathbf{X}_0)$, we employ the fact that a Markov process is characterized fully by the transition pdf and by an initial distribution $P_{in}(\mathbf{X}_0)$. The transition pdf of a continuous Markov process must fulfill the Chapman-Kolmogorov equation [2, 9]

$$P_c(\mathbf{X}, t + \tau | \mathbf{X}_0) = \int d\mathbf{X}' P_c(\mathbf{X}, \tau | \mathbf{X}') P_c(\mathbf{X}', t | \mathbf{X}_0) \quad \left(\mathbf{X}_0 \xrightarrow{t} \{\mathbf{X}'\} \xrightarrow{\tau} \mathbf{X} \right) \quad (36)$$

for any $\tau \geq 0$. In writing Eq. (36), we use that a process described by the Langevin Eqs. (24) is *homogeneous* provided the drift velocities are not explicitly time dependent: The conditional pdf, $P_c(\mathbf{X}, t | \mathbf{X}_0, t_0) = P_c(\mathbf{X}, t - t_0 | \mathbf{X}_0)$ of finding the system in \mathbf{X} at time t , given that it was in \mathbf{X}_0 at an earlier time t_0 , depends then only on the time difference. In fact, the moments in Eqs. (31-33) do depend only on the time difference τ .

For $\tau \ll \tau_a$, the Chapman-Kolmogorov equation simplifies to

$$P_c(\mathbf{X}, t + \tau | \mathbf{X}_0) = \int d\mathbf{X}' W_c(\mathbf{X}, \tau | \mathbf{X}') P_c(\mathbf{X}', t | \mathbf{X}_0) + o(\tau), \quad (37)$$

with the implication that any pdf $P(\mathbf{X}, t)$ can be constructed from an initial distribution $P_{in}(\mathbf{X})$ by repeated application of the short-time transition pdf [9]. Thus, the knowledge of W_c is sufficient to describe diffusion in multiple steps of τ . Explicitly (see Fig. 3)

$$P(\mathbf{X}, t) = \lim_{n \rightarrow \infty} \prod_{i=1}^{n-1} \int d\mathbf{X}_{i-1} W_c(\mathbf{X}, \tau | \mathbf{X}_{n-1}) W_c(\mathbf{X}_i, \tau | \mathbf{X}_{i-1}) P_{in}(\mathbf{X}_0), \quad (38)$$

with $\tau = t/n$. This path integral expression is the continuous analogue of a Markov chain used in (biased) Monte Carlo simulations to generate representative particle configurations. The n -fold product in Eq. (38) corresponds to an n -fold time-step forward integration in Eq. (29).

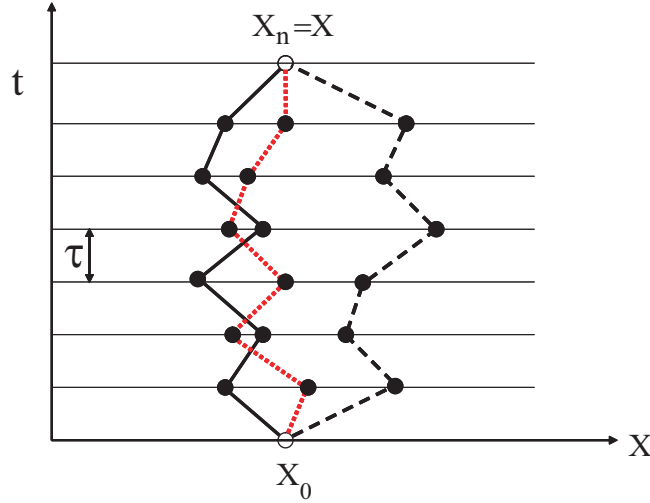


Fig. 3: Possible configuration paths between the fixed endpoints X_0 and X . For a Markovian process, one needs to sum over all paths.

It can be seen here that $P(\mathbf{X}, t)$ remains positive, if it was initially positive. Moreover, since W_c is strictly positive for non-zero τ , any configuration \mathbf{X} can be reached with non-vanishing probability density $P(\mathbf{X}, t)$, for whatever initial distribution has been chosen.

Differentiation of Eq. (37) with respect to τ , and insertion of Eq. (35) followed by two partial integrations, leads to the N -particle diffusion equation,

$$\frac{\partial}{\partial t} P_c(\mathbf{X}, t | \mathbf{X}_0) = -\nabla \cdot (\mathbf{v}^D(\mathbf{X}) P_c(\mathbf{X}, t | \mathbf{X}_0)) + D_0 \nabla^2 P_c(\mathbf{X}, t | \mathbf{X}_0), \quad (39)$$

with an explicit drift part invoking $\mathbf{v}^D(\mathbf{X})$, and a diffusive part invoking $D_0 > 0$. This is our searched for evolution equation for the (configurational) pdf, valid for sufficiently smooth density gradients so that $l_B |\nabla_i P(\mathbf{X}, t)| \ll 1$. In colloid science, this evolution equation is referred to as the *generalized Smoluchowski equation* (GSE) in the free-draining approximation (cf. lecture B1 by J. Dhont). Introducing the Smoluchowski differential operator,

$$\hat{\mathcal{O}}(\mathbf{X}) \equiv D_0 \nabla \cdot [\nabla - \beta \mathbf{F}(\mathbf{X})] \quad (40)$$

we can write the GSE more compactly as

$$\frac{\partial}{\partial t} P_c(\mathbf{X}, t | \mathbf{X}_0) = \hat{\mathcal{O}}(\mathbf{X}) P_c(\mathbf{X}, t | \mathbf{X}_0). \quad (41)$$

Alternatively, the GSE may be expressed in form of a continuity equation,

$$\frac{\partial}{\partial t} P(\mathbf{X}, t) + \sum_{i=1}^N \nabla_i \cdot \mathbf{j}_i(\mathbf{X}, t) = 0, \quad (42)$$

with probability currents

$$\mathbf{j}_i(\mathbf{X}, t) = -D_0 [\nabla_i - \beta \mathbf{F}_i(\mathbf{X})] P(\mathbf{X}, t). \quad (43)$$

The GSE is stochastically equivalent to the coupled positional Langevin Eqs. (24). It describes a continuous Markov process where all higher-order moments are of $o(\tau)$. For short times, it

reduces to the evolution Eq. (35) for $W_c(\mathbf{X}, \tau | \mathbf{X}_0)$. Using the explicit form of W_c , one easily shows for the polyadic conditional moments defined by

$$\langle \Delta \mathbf{X} \dots \Delta \mathbf{X} \rangle_0(\tau) \equiv \int d\mathbf{X} P_c(\mathbf{X}, \tau | \mathbf{X}_0) (\Delta \mathbf{X} \dots \Delta \mathbf{X}), \quad (44)$$

with $\Delta \mathbf{X} = \mathbf{X} - \mathbf{X}_0$, that these are identical to the moments derived from the positional Langevin equations.

General properties of the BD diffusion process for interacting particles are most easily explored on the basis of the GSE. We first notice that the canonical distribution function,

$$P_{eq}(\mathbf{X}) = \exp\{-\beta \Phi(\mathbf{X})\} / Z \quad \text{with} \quad Z = \int d\mathbf{X} \exp\{-\beta \Phi(\mathbf{X})\} \quad (45)$$

is a stationary solution of the GSE, that is $\hat{\mathcal{O}}P_{eq} = 0$. In addition, all stationary probability currents corresponding to P_{eq} are zero.

For the unbound suspension under consideration, we impose that $\Phi(\mathbf{X})$ increases sufficiently strongly for large r_i at least asymptotically, so that the configurational integral Z is finite. This implies that $P_{eq}(\mathbf{X}) \rightarrow 0$ and $\mathbf{j}_i(\mathbf{X}, t) \rightarrow 0$ for $|\mathbf{X}| \rightarrow \infty$, since $\Phi(\mathbf{X})$ acts like a reflecting barrier at infinity (natural boundary conditions, see [10]). It follows that probability is conserved: for any positive-valued $P_{in}(\mathbf{X})$ normalized to one, the solution $P(\mathbf{X}, t)$ of the GSE with $P(\mathbf{X}, 0) = P_{in}(\mathbf{X})$ remains positive and normalized for all subsequent times $t > 0$. Using an expansion of $P(\mathbf{X}, t)$ in terms of the left and right eigenfunctions of $\hat{\mathcal{O}}(X)$, one can show for natural boundary conditions (and $D_0 > 0$) that every solution of the GSE tends to the unique stationary solution $P_{eq}(\mathbf{X})$ in the course of time, irrespective of the initial distribution [1, 10]:

$$P(\mathbf{X}, t \rightarrow \infty) = P_{eq}(\mathbf{X}). \quad (46)$$

Eq. (46) holds true in particular for the conditional pdf, which is the fundamental solution of the GSE for a given initial delta-distribution at \mathbf{X}_0 . Using Eq. (41), we may write the *formal* solution for P_c as

$$P_c(\mathbf{X}, t | \mathbf{X}_0) = \exp\{t \hat{\mathcal{O}}(\mathbf{X})\} \delta(\mathbf{X} - \mathbf{X}_0), \quad (47)$$

which shows explicitly that the time-independence of $\hat{\mathcal{O}}(\mathbf{X})$ is a consequence of the temporal homogeneity of the process $\mathbf{X}(t)$.

3.3 Simulation details

So far we have explored the theoretical basis of the BD simulation method. We proceed to describe how an actual simulation is performed in the free-draining approximation. The BD simulation scheme has various concepts in common with Molecular Dynamics and Monte-Carlo simulations [11]. For a more detailed account of these common concepts, we can thus refer to lecture B3 of R.G. Winkler, and lecture B2 of G. Vlieghart.

Let us focus on the Brownian Dynamics of a quiescent suspension of spherical particles interacting by a given soft pair potential $u(r)$. The suspension we wish to describe in the simulation is supposed to be in an equilibrium fluid state.

Typical BD simulations in the free-draining approximation are performed for $N = O(10^2 - 10^3)$ particles placed in a cubic box of length $L = (N/\rho)^{1/3}$, where ρ is the particle number

density. In order to minimize effects originating from the small sample size, periodic boundary conditions are applied, i.e. the basic simulation box is periodically replicated in all three spatial directions. As a particle moves out of the simulation box, an image moves in at the opposite side of the box to replace it. Due to the periodic boundary conditions, density fluctuations of wavelengths larger than L are suppressed. However, the influence of the finite box size is small for $N > 100$, provided the particles are in an isotropic fluid phase. A BD simulation run usually starts with the centers of the particles placed regularly on a lattice. Quite often a fcc lattice is used for the starting configuration. Then the particle number is $N = 4m^3$, where m is an integer, since the fcc unit cell consists of four particles. Alternatively, one may start from a configuration obtained from a previous simulation with similar system parameters. In a subsequent *equilibration run*, about $10^4 - 10^5$ configurations (or BD time-steps τ) are generated to allow the system to reach its equilibrium state. A BD time-step consists of the simultaneous displacement of all N particles according to Ermak's integration scheme in Eq. (29). The actual number of time-steps needed for equilibration depends on the selected initial configuration, particle density, temperature, softness of the potential et cetera. The melting of the initial fcc lattice (cf. Fig. 4), and the approach towards equilibrium can be monitored by the translational order parameter [11]

$$\rho(\mathbf{q}) \equiv \frac{2}{N(N-1)} \sum_{i < j}^N \cos(\mathbf{q} \cdot [\mathbf{r}_i - \mathbf{r}_j]) , \quad (48)$$

where \mathbf{q} is a reciprocal fcc lattice vector (for instance, $\mathbf{q} = (2\pi d^{-1})(-1, 1, -1)$ with the fcc lattice constant d), and by the configurational energy per particle,

$$e = \frac{1}{Nk_B T} \sum_{i < j}^N u(|\mathbf{r}_i - \mathbf{r}_j|) . \quad (49)$$

A proper equilibration is ensured when steady mean values of e and $\rho(\mathbf{q})$ have been reached, up to small fluctuations of $O(N^{-1/2})$. For a crystalline solid, $\rho(\mathbf{q})$ is of the order of one whereas $\langle \rho(\mathbf{q}) \rangle = 0$ in the fluid state. After equilibration, the actual sampling is done in a *production run* where typically another few $10^4 - 10^5$ time-steps are generated. Static equilibrium and dynamic transport properties of interest can, in principle, be calculated from configurations sampled during the production run.

The computationally most expensive parts in the free-draining simulation scheme are firstly the calculation of the direct inter-particle forces and, secondly but less severely, the calculation of the random displacements for each configuration. For a sufficiently short-range pair potential, one can approximate $u(r_{ij} > r_c) = 0$, with a potential cutoff distance r_c which is significantly smaller than $L/2$. Then a particle interacts at most with $(N - 1)$ neighboring particles in the central simulation cell or in the next-neighbor image cells, so that at most $N(N - 1)$ pair forces need to be considered (*minimum image convention*, see Fig. 4). The force calculations are speeded up using neighbor lists with so-called Verlet shells surrounding the potential-cutoff sphere of each particle in the central simulation box, to reduce the force updating. For larger systems with $N \geq 1000$, it is preferential to use a regular cell division of the central box with linked lists [11]. With these tools, a $O(N)$ scaling of the computation time can be reached, in contrast to the lengthy $O(N^2)$ operations required in a 'brute-force' calculation. In systems with long-range Coulomb interactions, each particle interacts in principle with all particles in the central box and all images. The computational effort is thus of $O(N^2)$ already for the central

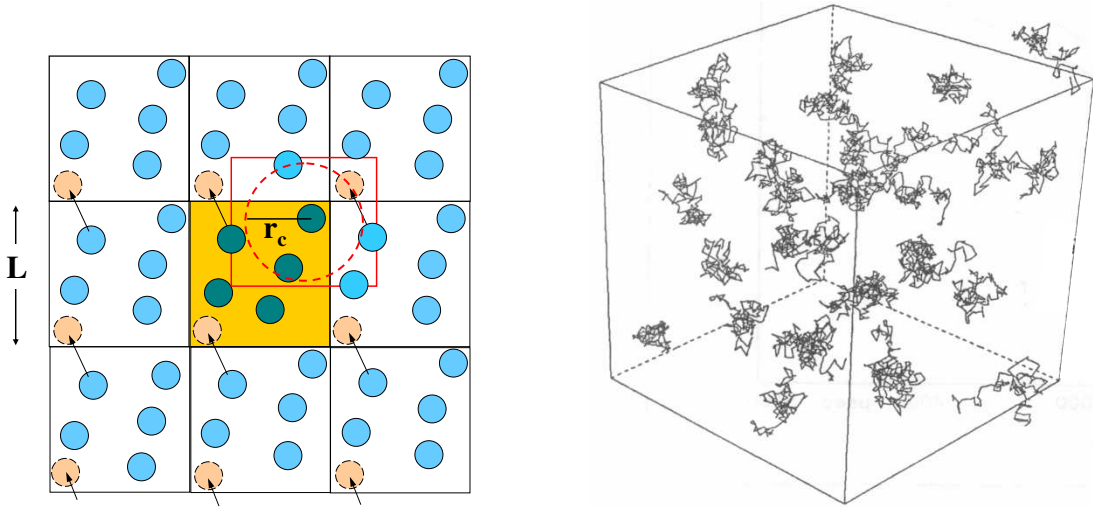


Fig. 4: *Left: periodic boundary conditions and minimum image convention cell with inscribed potential-cutoff sphere (dashed circle). Right: melting of an initial fcc configuration ($N = 32$ particles at $t = 125\tau$). Not shown are the trajectories of incoming image particles.*

box. In this more demanding case one needs to resort to an Ewald summation technique for periodic systems, to sum an infinite number of pair interactions. With the most advanced variants of this technique at hand, the summation can be scaled down to an $O(N \log N)$ calculation [12]. The random displacements in Eq. (29) require, at any time-step and for all three spatial directions, the generation of a Gaussian-distributed random number n of zero mean and unit variance. With standard quasi-random number generators for uniformly distributed numbers ξ on the range $(0, 1)$, the standard Box-Müller method may be invoked to create Gaussian random numbers [11, 13]. However, on the level of the first-order Ermak algorithm, it is not necessary to use Gaussian-distributed random numbers [14, 15]. Only the first and second moments are needed, which can be equally well obtained, and less expensively, using a random number R in place of n , constructed from the uniformly distributed random number ξ according to

$$R = \sqrt{12} \left(\xi - \frac{1}{2} \right). \quad (50)$$

One easily confirms that R has the same first two moments as n , and that all odd moments of its distribution are zero.

The basic time-step τ in Ermak's scheme should be chosen as large as possible for an efficient sampling of configuration space, but small enough that the forces remain essentially constant. Typical values are in the range $\tau/\tau_a \sim 0.5 \times 10^{-4} - 0.5 \times 10^{-2}$. In dense systems and in systems with steeply repulsive pair interactions, smaller time-steps are required, whereas larger time-steps may be used for less strongly correlated particles.

An important static property, which can be calculated in a BD simulation, is the radial distribution function $g(r)$. This function gives the probability of finding a second particle a distance r from a given one, relative to the probability expected for a completely random distribution at the same density [5]. In other words, $\rho(r) \equiv \rho g(r)$ is the local density around a given particle, as a function of the distance from that particle. For a homogeneous and isotropic fluid, $g(r)$

may be calculated, for distances $r < r_c$ and in three dimensions, from

$$g(r) = \left\langle \frac{1}{N} \sum_{i=1}^N \frac{\Delta N_i(r, r + \Delta r)}{\rho 4\pi r^2 \Delta r} \right\rangle_M, \quad (51)$$

where the arithmetic average $\langle \dots \rangle_M$ extends over M configurations selected from the BD production run. The M configurations should be separated by the order of ten time-steps to be statistically independent, with the memory on a previously selected configuration being lost. This is important for dense systems where a configuration changes only little during an elementary time-step τ . For a given configuration, $\Delta N_i(r, r + \Delta r)$ is the number of particles with centers in a spherical shell of radius r and thickness $\Delta r \ll r$, with particle i in its center. With the assumed pairwise additivity of the configurational energy, all equilibrium static properties like the osmotic pressure and the colloidal internal energy, can be expressed in $g(r)$ and no higher-order distribution functions are required.

In real experiments, $g(r)$ can be measured directly only in video microscopy experiments on quasi-two-dimensional layers of large colloidal particles. In the bulk of suspensions, information on $g(r)$ is obtained only indirectly through static scattering experiments where in an isotropic fluid phase the static structure factor,

$$S(q) = 1 + \rho \int d\mathbf{r} (g(r) - 1) \exp\{i \mathbf{q} \cdot \mathbf{r}\}, \quad (52)$$

is determined, which is essentially the Fourier transform of $g(r)$. In a simulation, $g(r)$ is obtained only up to the cutoff distance r_c . Therefore, instead of attempting to obtain $S(q)$ through Fourier-inverting the simulated $g(r)$, it is advisable to compute $S(q)$ directly according to

$$S(q) = 1 + \frac{2}{N} \left\langle \sum_{i < j}^N \cos(\mathbf{q} \cdot \mathbf{r}_{ij}) \right\rangle_M. \quad (53)$$

To be compatible with the periodic boundary conditions, the scattering wavevector \mathbf{q} of modulus q is restricted to discrete values $\mathbf{q} = (2\pi/L)(n_x, n_y, n_z)$, with $\mathbf{q} = 0$ excluded, where L is the size of the box and n_x, n_y and n_z are integers. The statistics in calculating $S(q)$ is improved for an isotropic system by averaging over differently oriented wavevectors of equal magnitude q .

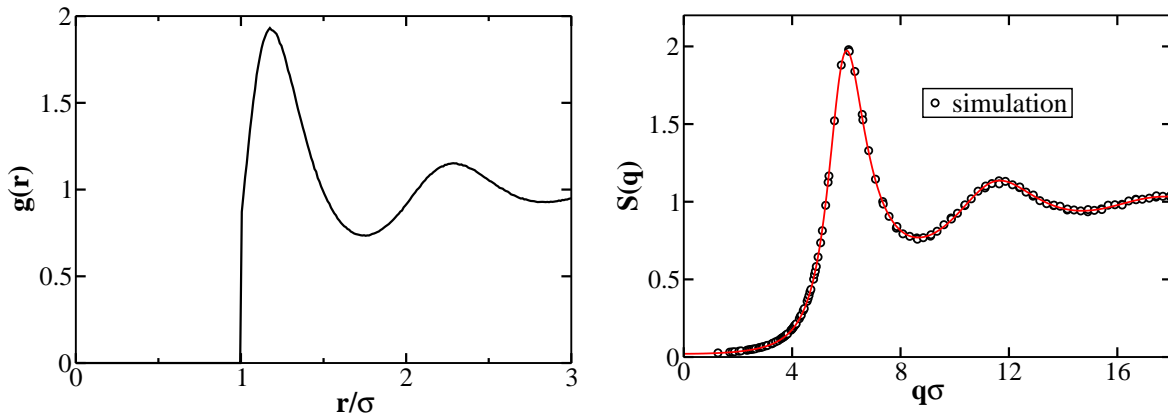


Fig. 5: Left: BD simulation result for $g(r)$ of charged colloidal proteins, using $N = 500$ and 860 particles. Right: corresponding simulated static structure factor. Redrawn from [16].

Fig. 5 includes BD simulation results of $g(r)$ and $S(q)$ typical for dense suspensions of charged colloidal spheres. The spheres interact by an effective pair potential which is a sum of a hard-core repulsion, and a soft and longer-range screened Coulomb potential part of the form [3],

$$\beta u_S(r) = L_B Z^2 \left(\frac{e^{\kappa a}}{1 + \kappa a} \right)^2 \frac{e^{-\kappa r}}{r}, \quad r > 2a, \quad (54)$$

with Bjerrum length $L_B = e^2/(\epsilon k_B T)$, electrostatic screening parameter κ and effective particle charge Z in units of the elementary charge e . The system parameters have been selected to describe qualitatively charged globular proteins (apoferritin) of diameter $\sigma = 13.8$ nm dispersed in water at room temperature (with $L_B = 0.71$ nm), for a quite large particle volume fraction $\phi = (4\pi/3)\rho a^3$ of 0.33 [16]. The jump in $g(r)$ at $r = \sigma$ is due to the hard-sphere potential part which is not negligible for such a large volume fraction. How hard-body interactions are included into BD simulations will be discussed in the following subsection.

The static equilibrium properties $g(r)$ and $S(q)$ are not affected by HI, in contrast to the mean-square displacement $W(t)$ defined in Eq. (10). From a BD production run, $W(t)$ may be determined as (t must be a multiple of τ)

$$W(t) = \left\langle \frac{1}{6N} \sum_{i=1}^N [\mathbf{r}_i(t + t_0) - \mathbf{r}_i(t_0)]^2 \right\rangle_{t_0}. \quad (55)$$

The angular brackets refer to an arithmetic average over a number of starting times t_0 . These initial times are taken from the same long production run at well-separated time spacings ($\geq \tau_a$). For a stationary system, $W(t)$ is independent of t_0 . Hence averaging over the initial times helps to improve the signal-to-noise ratio of the MSD. Another dynamic property influenced by HI is the dynamic structure factor $S(q, t)$, defined by

$$S(q, t) = \left\langle \frac{1}{N} \sum_{l,p=1}^N \exp\{i \mathbf{q} \cdot (\mathbf{r}_l(t + t_0) - \mathbf{r}_p(t_0))\} \right\rangle_{t_0}. \quad (56)$$

The dynamic structure factor is the time-dependent generalization of the static structure factor, with $S(q, t = 0) = S(q)$. It describes time auto-correlations in the \mathbf{q} -th Fourier component of local microscopic density fluctuations [3]. Free-draining simulation results for $W(t)$ and $S(q, t)$ will be discussed in the following subsection.

3.4 Simulation of particles with hard-body interaction

The Ermak integration scheme discussed above assumes a continuous deterministic force field $\mathbf{F}_i(\mathbf{X}) = -\sum_{l \neq i} \nabla_i u(r_{il})$. It becomes troubled when systems with significant hard-body interaction parts are considered. The pair potential in these systems is the sum of a hard-core part, $u_{HC}(r)$, of diameter $\sigma = 2a$, and a longer-range soft part, $u_S(r)$. The soft part may be attractive, zero or so weakly repulsive that there is a significant probability to find two or more spheres in contact. The fact that two spheres can not interpenetrate is expressed by the zero relative radial flux boundary conditions [17]

$$\hat{\mathbf{r}}_{il} \cdot [\mathbf{j}_i(\mathbf{X}, t) - \mathbf{j}_l(\mathbf{X}, t)]|_{r_{il}=\sigma^+} = 0, \quad (57)$$

for two spheres i and l in contact. Here, $\hat{\mathbf{r}}_{il} = \mathbf{r}_{il}/r_{il}$ with $\mathbf{r}_{il} = \mathbf{r}_i - \mathbf{r}_l$, is the unit vector pointing from the center of sphere l to the center of sphere i , and $\mathbf{j}_i(\mathbf{X}, t)$ is the probability current as

defined in Eq. (43). Since the relative radial flux is zero at contact, the particle trajectories of i and l must be reflected.

Note that genuine hard spheres are described by a GSE with all $\{\mathbf{F}_i\}$ equal to zero, augmented by the exact zero relative flux boundary conditions. Ermak's algorithm (29) is per se not applicable to hard spheres since it requires finite and continuous forces. One possibility to deal with singular hard-body interactions within Ermak's scheme is to approximate $u_{HC}(r)$ by a soft potential of the form

$$u(r) = k_B T \left(\frac{\sigma}{r} \right)^m, \quad (58)$$

where m is a sufficiently large integer (cf. Fig. (6)). The soft-potential approximation for the particular exponents $m = 32$ and 64 has been used in free-draining BD simulations of hard spheres [18, 19]. In case of dense systems, however, large values of the inter-particle force are produced which make it necessary to use very small time-steps. Otherwise, unrealistically large displacements are obtained resulting in possible particle overlaps.

For dense systems, potential-free methods have been proposed to account for the zero-flux boundary conditions. One frequently used method [20, 21] is to perform first a one-step displacement of all N spheres according to Ermak's scheme. The configuration is then checked for overlapping particles. All overlapping pairs of spheres are symmetrically displaced along their lines of center so that they are right in contact afterwards (cf. Fig. 6). Subsequently, Ermak's one time-step evolution is applied again. This simple approximate algorithm cannot resolve all overlaps, unless computationally expensive small time-steps are used, since the overlap corrections are done in a pairwise fashion and may create new overlaps.

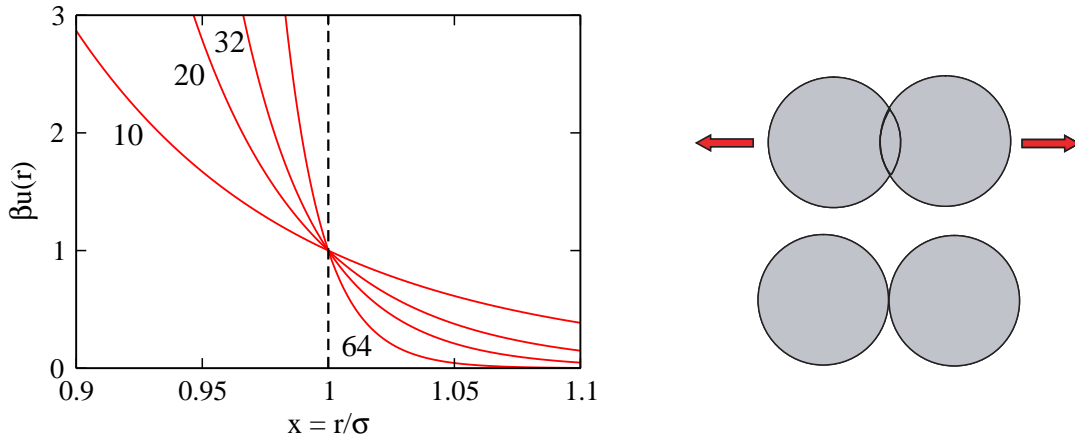


Fig. 6: Left: soft pair potential approximation, Eq. (58), for exponents m as indicated. Right: potential-free algorithm to correct for sphere overlap.

A totally different method to generate the zero relative radial flux boundary conditions has been proposed that uses a binary elastic collision correction to adjust the positions after an overlap detection [22]. This correction scheme is similar in spirit to a Molecular Dynamics simulation of hard spheres and eliminates *all* residual overlaps. It has been applied to explore the free-draining dynamics of Brownian hard spheres, for concentrations even above the melting transition [23]. For a related method which has been suggested to cope with hard-body interactions, see also [24].

Yet another tool to deal with hard spheres, and particles with steep short-range repulsions, is the so-called *smart Brownian Dynamics method* [25–29]. This is actually a *biased Monte*

Carlo method where trial moves of the particles are sampled according to Brownian Dynamics, i.e. using the Ermak scheme. In smart BD, the trial moves are biased in the direction of the acting force, that is in direction of probable moves. Thus, a higher acceptance rate may be expected than for the uniform and unbiased stochastic moves made in the standard Metropolis Monte Carlo scheme. The smart BD method is based on the following fact: for the dynamics described by the GSE with zero radial flux boundary conditions on the particle surfaces, the detailed balance relation

$$P_c(\mathbf{X}_j, \tau | \mathbf{X}_i) P_{eq}(\mathbf{X}_i) = P_c(\mathbf{X}_i, \tau | \mathbf{X}_j) P_{eq}(\mathbf{X}_j), \quad (59)$$

is obeyed by the exact transition pdf, P_c , for all times $\tau > 0$. The physical content of this microreversibility relation is that, in equilibrium, a transition from configurational state $i = \mathbf{X}_i$ to state $j = \mathbf{X}_j$ during τ , is equally probable as the inverse transition $j \rightarrow i$. Detailed balance is a sufficient, but not necessary, condition on P_{eq} in Eq. (59) to be a stationary solution of the GSE. This follows directly from integrating the detailed balance relation with respect to \mathbf{X}_j .

The validity of detailed balance ensures, for natural boundary conditions at infinity, that configurations created according to the GSE, or its associated positional Langevin equations, form a Markov sequence which becomes equilibrium distributed after an equilibration period (cf. Eq. (46)). A proof of the validity of detailed balance in Brownian Dynamics is most simply obtained from Eq. (47), with the Smoluchowski operator $\hat{O}(\mathbf{X})$ expressed in terms of its left and right eigenfunctions [5, 10].

Using the Ermak updating scheme amounts to replace P_c , in eq. (59), by its *known* short-time approximation $W_{i \rightarrow j} = W_c(\mathbf{X}_j, \tau | \mathbf{X}_i)$. This replacement implies a strong violation of detailed balance when the move $i \rightarrow j$ results in particle overlap: the left-hand side of this relation is positive since $W_{i \rightarrow j} > 0$ even when an overlap configuration j is reached. In contrast, the right-hand-side side is zero since $P_{eq}(\mathbf{X}_j) = P_{eq}(j) = 0$ for an overlap configuration j . The transition pdf $W_{i \rightarrow j}$ depends on the initial state i through the initial drift vector. Hence it is non-symmetric in i and j . It is referred to as the stochastic matrix underlying the Markov sequence.

To repair detailed balance even for longer time-steps τ , where non-physical moves within the Ermak scheme are likely, we replace $W_{i \rightarrow j}$ by a corrected transition pdf, $\widetilde{W}_{i \rightarrow j}$, determined for $i \neq j$ by

$$\widetilde{W}_{i \rightarrow j} \equiv \begin{cases} W_{i \rightarrow j}, & \text{if } P_{eq}(j) W_{j \rightarrow i} \geq P_{eq}(i) W_{i \rightarrow j} \\ W_{j \rightarrow i} \cdot \frac{P_{eq}(j)}{P_{eq}(i)}, & \text{if } P_{eq}(j) W_{j \rightarrow i} < P_{eq}(i) W_{i \rightarrow j}. \end{cases} \quad (60)$$

One can easily convince oneself that \widetilde{W}_{ij} obeys detailed balance even in the case of particle overlap. We can write $\widetilde{W}_{i \rightarrow j}$ alternatively as $\widetilde{W}_{i \rightarrow j} = Q_{i \rightarrow j} W_{i \rightarrow j}$, with the acceptance probability given by

$$Q_{i \rightarrow j} = \min \left[1, \frac{\exp\{-\beta\Phi(j)\}}{\exp\{-\beta\Phi(i)\}} \cdot \frac{W_{j \rightarrow i}}{W_{i \rightarrow j}} \right]. \quad (61)$$

It is clear that $Q_{i \rightarrow j} = 1$ for any move $i \rightarrow j$ where the short-time transition pdf satisfies detailed balance. The calculation of $Q_{i \rightarrow j}$ does not require the knowledge of the high-dimensional configurational integral Z .

In principle, it is not necessary to move all particles simultaneously from the N -particle state i to the state j . Instead, one could equally well move the N particles consecutively using the

Ermak scheme. To comprehend this recall from the factorization of $W_c(\mathbf{X}_j, \tau | \mathbf{X}_i)$ in Eq. (34) that during a time-step τ , each particle moves independently from the others in the same 'static' surrounding (i.e., initial configuration i). Hence it is legitimate to replace the N -particle short-time transition pdf's in Eqs. (60) and (61) by the corresponding single-particle transition pdfs. We are now in the position to formulate the structure chart of the smart BD algorithm for trajectories generated according to \widetilde{W}_{ij} :

- (a) Select a non-overlapping configuration $\mathbf{X}_0 = (\mathbf{r}_{10}, \dots, \mathbf{r}_{N0})$.
- (b) Choose a random permutation of $\{1, \dots, N\}$ and keep it fixed until all particles have been moved once.
- (c) Sample a new position \mathbf{r}_1 of particle 1 according to the Ermak scheme.
- (d) Accept the tentative move with probability $Q_{i \rightarrow j}$ by comparison with a random number ξ sampled uniformly in $(0, 1)$. If $\xi \leq Q_{i \rightarrow j}$, the move is accepted. Otherwise, go back to the old state \mathbf{r}_{10} and count this state once more before a new move is attempted.
- (e) Repeat steps (3-4) for all remaining particles $2, \dots, N$.
- (f) Time is advanced after each particle has had a trial move.

According to Eq. (61), the crucial Monte Carlo decision (d) becomes particularly simple for pure hard spheres [27]: a move is accepted if there is no resulting overlap, and rejected otherwise. Note that the old state has to be counted again for a rejected move, since there is a non-zero probability for a transition $i \rightarrow i$, and this has to be given appropriate weight.

By its very construction, the smart BD algorithm fulfills detailed balance under all conditions so that the approach to thermal equilibrium is ensured. Hence correct equilibrium averages, like Eq. (51) for $g(r)$, are obtained after equilibration even when a large τ has been selected. However, if the generated trajectories are used not only to sample the configuration space efficiently, but to calculate dynamic properties like the mean-square displacement, then the smart BD algorithm becomes exact in the limit $\tau \rightarrow 0$ only. This follows from $Q_{i \rightarrow j} \rightarrow 1$ for $\tau \rightarrow 0$, as may be noted from Eqs. (34) and (61). In this limit, $W_{i \rightarrow j}$ satisfies detailed balance and every tentative configuration will be accepted. Then the smart BD and Ermak BD schemes are truly the same. Smart BD, however, offers practical advantages over the Ermak procedure since it allows for appreciable larger time-steps, where the basic BD procedure becomes unreliable or even non-physical. The smart BD algorithm can be straightforwardly extended to systems of hydrodynamically interacting particles [30].

Smart BD results for the mean-square displacement, $W(t)$, of hard spheres in the free-draining approximation measured relative to the MSD, $D_0 t$, of non-interacting spheres, and for the dynamic structure factor, $S(q, t)$, at a fixed wavenumber $q = 9.8/\sigma$, are depicted in Fig. 7. At short times, $\tau_B \ll t \ll \tau_a$, a probe particle does not yet experience the mean influence of direct interactions with neighboring particles. Therefore, $W(t)$ grows initially linear in time according to $W(t) = D_S t$, with the short-time self-diffusion coefficient, D_S , equal to D_0 in the free-draining approximation. Unlike the direct interactions, the slowing influence of HI is felt instantaneously, giving rise to $D_S < D_0$ when HI is included. At intermediate times $t \sim \tau_a$, the dynamic 'cage' formed around the probe sphere by neighboring spheres becomes distorted from its equilibrium spherical symmetry so that the probe particle is now additionally hindered in its diffusion by direct interaction forces. The cage distortion leads to a sub-linear time dependence of $W(t)$ at times $t \sim \tau_a$. This sub-linear time regime is most clearly resolved by plotting

the ratio $W(t)/(D_0 t)$ versus time. At long times $t \gg \tau_a$, the probe sphere has experienced many independent interaction events with neighboring particles, which implies again a linear time dependence according to $W(t) = D_L t$, quantified now by the long-time self-diffusion coefficient D_L . The long-time coefficient is smaller than D_S for any form of direct interaction. Consequently, $W(t)/(D_0 t)$ in the free-draining approximation decays from one for short times towards the long-time ratio D_L/D_0 . As can be noticed from Fig. 7, this ratio gets smaller for increasing particle concentration.

The monotonic decay of the dynamic structure factor, $S(q, t)$, shown in the right part of Fig. 7, from its initial value $S(q)$ towards the final value zero, exemplifies a general rule stating that any configurational one-time *auto*-correlation function is decaying strictly monotonically in time when observed on the Brownian Dynamics time scale of $t \gg \tau_B$ [5]. For any given q , the decay of $S(q, t)$ becomes slower with increasing concentration.

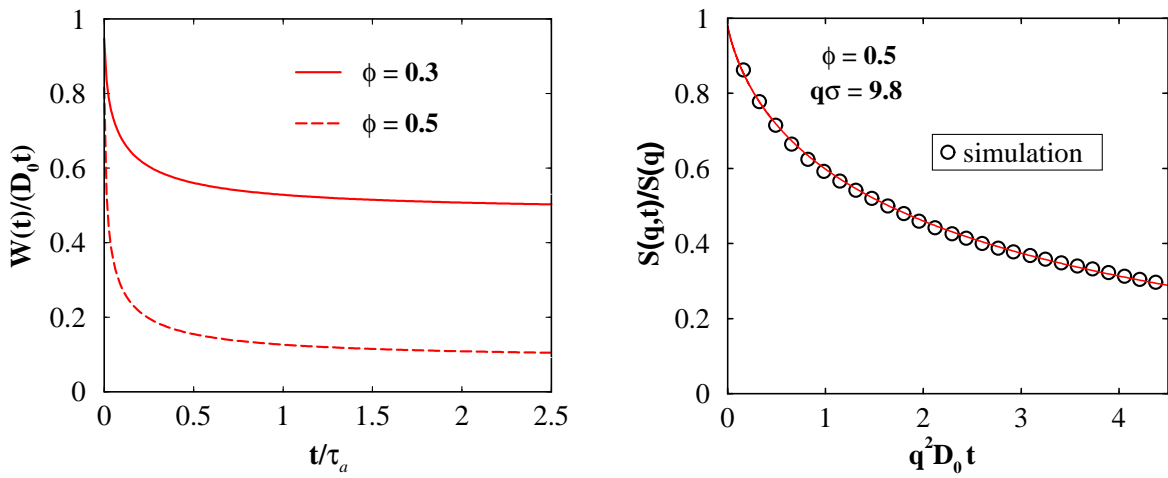


Fig. 7: Left: smart BD results for the mean-square displacement of hard spheres in free-draining approximation (redrawn from [31]). Particle volume fractions ϕ as indicated. Right: dynamic structure factor of hard spheres versus reduced time (redrawn from [32]).

4 Brownian Dynamics simulations with hydrodynamic interactions

In the following we describe how the free-draining BD simulation scheme can be extended to account for hydrodynamic interaction effects. HI are in general not pairwise-additive, they are long-range, decaying like $1/r$ in the inter-particle distance r , and they diverge for certain types of motion when particles approach each other very closely (lubrication effects). These three properties make their numerical treatment difficult. As we will see, the implementation of HI into the Ermak scheme requires in principle $O(N^3)$ matrix inversions, and the computation of correlated forces between different particles to satisfy the fluctuation-dissipation relation. The computational bottleneck is thus the incorporation of HI, and not the force calculation as in the free-draining limit. To date standard BD simulations with HI are therefore limited to small systems of particle numbers $32 \leq N \leq 256$.

There are mathematical subtleties related to the proper definition of Langevin equations with HI included [1, 2, 33]. For this reason, we will derive the extension of Ermak's finite difference

scheme starting from the generalized Smoluchowski diffusion equation. The GSE equation for the configurational pdf, $P(\mathbf{X}, t)$, is unequivocally defined even when HI is included.

4.1 Hydrodynamic interactions of spheres

On colloidal time scales $t \gg \tau_\eta \sim \tau_B$, the motion of the solvent can be described by the so-called creeping flow or Stokes equation [34, 35],

$$-\nabla p(\mathbf{r}) + \eta_0 \nabla^2 \mathbf{u}(\mathbf{r}) = 0, \quad \nabla \cdot \mathbf{u}(\mathbf{r}) = 0, \quad (62)$$

where $\mathbf{u}(\mathbf{r})$ is the fluid velocity at point \mathbf{r} , and $p(\mathbf{r})$ is the pressure field (cf. lecture B1 of J. Dhont). In addition, boundary conditions on the particle surfaces and at infinity must be specified. Commonly, it is assumed that the solvent sticks perfectly to the particle surfaces. Stick boundary conditions can be justified experimentally for colloidal particles where $a \geq 30$ nm [36]. For a quiescent suspension without externally imposed flow, $\mathbf{u}(\mathbf{r})$ vanishes at infinity. Eq. (62) is the linearized and stationary form of the Navier-Stokes equation. Linearization is justified since the Reynolds number, Re , in quiescent colloidal systems is very small. To give an example, $Re = a\rho_s v_{th}/\eta_0 \approx 5.4 \times 10^{-5}$ for spheres of radius 100 nm suspended in water at room temperature and driven thermally by Brownian motion where $v_{th} = (3k_B T/m)^{1/2}$. For a time resolution $t \gg \tau_\eta$, viscous shear waves and sound waves created by unsteady particle motions have decayed away over distances where the particles are correlated². Therefore colloidal flow can be considered as quasi-incompressible and time-independent. Note that Eq. (62) expresses a force-balance between pressure and viscous forces.

Consider now a quiescent and unbound suspension of N identical colloidal spheres in a Newtonian fluid which are allowed to rotate freely (i.e. no external torques applied). Since the creeping flow equation is linear and stationary, the translational velocity, \mathbf{v}_i , of a sphere i is linearly and instantaneously related to the hydrodynamic forces, $\{\mathbf{F}_j^h\}$, exerted on the surfaces of the N spheres through their friction with the surrounding fluid (cf. Fig. 8),

$$\mathbf{v}_i = -\beta \sum_{j=1}^N \mathbf{D}_{ij}(\mathbf{X}) \cdot \mathbf{F}_j^h. \quad (63)$$

The tensors \mathbf{D}_{ij} are referred to as translational *hydrodynamic diffusivity tensors* or likewise, after division by $k_B T$, as translational hydrodynamic mobility tensors. These tensors are complicated functions of all colloid positions. They form the elements of a symmetric and positive definite $3N \times 3N$ diffusivity matrix

$$\mathbf{D}(\mathbf{X}) = \begin{pmatrix} \mathbf{D}_{11} & \mathbf{D}_{12} & \dots & \mathbf{D}_{1N} \\ \mathbf{D}_{21} & \mathbf{D}_{22} & \dots & \mathbf{D}_{2N} \\ \vdots & \vdots & \ddots & \vdots \\ \mathbf{D}_{N1} & \mathbf{D}_{N2} & \dots & \mathbf{D}_{NN} \end{pmatrix}. \quad (64)$$

The positivity of the matrix \mathbf{D} is a consequence of the friction-dominated motion of colloidal particles which gives rise to a steady irreversible dissipation of their kinetic energy into heat

²At times $t \sim \tau_\eta$, a linear inertial term $\rho_s \partial \mathbf{u} / \partial t$ must be added to the lhs of Eq. (62). This term gives rise to the long-time tail noted in Eq. (22).

according to [35]:

$$\dot{E}_{kin} = \sum_{i=1}^N \mathbf{F}_i^h \cdot \mathbf{v}_i = -\beta \sum_{i,j=1}^N \mathbf{F}_i^h \cdot \mathbf{D}_{ij} \cdot \mathbf{F}_j^h < 0 . \quad (65)$$

Analytical calculations of the diffusivity tensors are difficult even in case of spheres, and have been achieved fully only on a pairwise-additive level, mainly in form of expansions in the inverse distance, a/r_{ij} , between two spheres. Hereby one disregards the influence of other spheres on the HI between a given pair of spheres, an approximation which is valid only for large inter-particle spacings. The N -sphere diffusivity tensors can be written as the sum [5, 34]

$$\mathbf{D}_{ij}(\mathbf{X}) = \mathbf{D}_{ij}^{RP}(\mathbf{r}_{ij}) + \Delta \mathbf{D}_{ij}(\mathbf{X}) , \quad (66)$$

consisting of a far-field part, referred to as Rotne-Prager (RP) approximation [37]

$$\mathbf{D}_{ij}^{RP}(\mathbf{r}_{ij}) = \delta_{ij} D_0 \mathbf{1} + (1 - \delta_{ij}) D_0 \left\{ \frac{3}{4} \left(\frac{a}{r_{ij}} \right) [\mathbf{1} + \hat{\mathbf{r}}_{ij} \hat{\mathbf{r}}_{ij}] + \frac{1}{2} \left(\frac{a}{r_{ij}} \right)^3 [\mathbf{1} - 3 \hat{\mathbf{r}}_{ij} \hat{\mathbf{r}}_{ij}] \right\} , \quad (67)$$

which is the long-distance expansion of $\mathbf{D}_{ij}(\mathbf{X})$ up to $O(a/r_{ij})^3$, and a complicated near-field part, $\Delta \mathbf{D}_{ij}(\mathbf{X})$, which accounts for all remaining contributions. Here, D_0 is defined as in Eq. (12), with $\zeta_0 = 6\pi\eta_0 a$ for stick boundary conditions. The near-field part includes all higher-order two-body as well as all many-body contributions, and it becomes increasingly important with smaller particle separations. It also accounts for the hydrodynamic lubrication effect: the relative hydrodynamic mobility of two spheres must vanish at contact, proportional to $h = (r_{ij} - 2a)$ for spheres i and j in relative motion along their line of centers [35]. This singular behavior arises since the solvent, which sticks to the particle surfaces, must be squeezed out of the narrow gap (cf. Fig. 8). Lubrication effects are relevant for surface-to-surface distances $h/a \sim 10^{-2}$. However, for very small $h \sim 10^{-8}$ cm, the mean free path of solvent molecules will be of the order of the nearest surface-to-surface distance so that some slip is introduced. Therefore, the no-slip boundary condition between surface and solvent, and the continuum picture of the solvent underlying Eq. (62) and lubrication theory, can not be exactly true for an actual physical system.

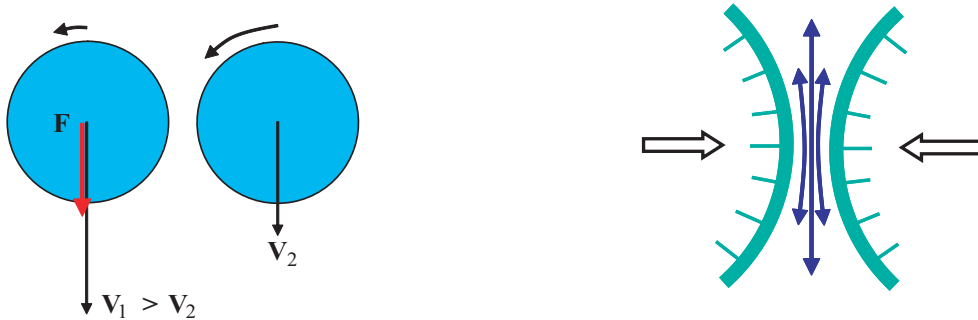


Fig. 8: *Left: hydrodynamic interactions (HI) between colloidal spheres. Right: singular lubrication forces in the narrow fluid gap between two approaching spheres close to contact.*

The RP form of $\mathbf{D}_{ij}(\mathbf{X})$ is a valid approximation for dilute systems consisting of particles which repel each other strongly over larger distances, for example like-charged colloidal poly-ions. This approximation is not applicable to hard spheres since two hard spheres are likely found in

near contact. Two convenient features of the RP approximation are firstly, that it preserves the positivity of the exact diffusivity matrix for all non-overlap configurations, and secondly, that the diffusivity tensors are divergence-free in RP approximation,

$$\nabla_j \cdot \mathbf{D}_{ij}^{RP}(\mathbf{r}_{ij}) = 0 . \quad (68)$$

The first feature is a prerequisite to guarantee convergence to equilibrium of the BD scheme. The second property amounts to a significant reduction in computation time. It should be emphasized, however, that in general \mathbf{D}_{ij} is not divergence-free since $\nabla_j \cdot \Delta \mathbf{D}_{ij} \neq 0$.

In BD simulations of polymer solutions, a polymer is often modelled as a linear chain consisting of spherical beads of *hydrodynamic* radius a , linked together consecutively by some sort of continuous spring-potential $u(r)$ [38, 39]. For numerical tractability, the HI between the beads are commonly described in RP approximation. Moreover, to avoid the use of excluded volume interactions with their troublesome implications (e.g., very small time-steps and non-negligible near-field HI effects), one allows for some overlap of the beads. This requires a regular extension of \mathbf{D}_{ij}^{RP} into the region $r_{ij} < 2a$, which is non-singular at $r_{ij} = 0$ and positive definite for all bead configurations. Such an extension is provided by the Rotne-Prager-Yamakawa tensor, \mathbf{D}_{ij}^{RPY} , defined as $\mathbf{D}_{ij}^{RPY} = \mathbf{D}_{ij}^{RP}$ for $r_{ij} > 2a$, and [37, 40, 41]

$$\mathbf{D}_{ij}^{RPY}(\mathbf{r}_{ij}) = D_0 \left\{ \left(1 - \frac{9r_{ij}}{32a} \right) \mathbf{1} + \frac{3r_{ij}}{32a} \hat{\mathbf{r}}_{ij} \hat{\mathbf{r}}_{ij} \right\} \quad \text{if } i \neq j \text{ and } r_{ij} < 2a . \quad (69)$$

While this extension amounts to an inconsistent mix of direct and hydrodynamic interactions, it preserves the positivity of $\mathbf{D}(\mathbf{X})$, and the validity of $\nabla_j \cdot \mathbf{D}_{ij}^{RPY} = 0$ even for overlapping chain conformations.

4.2 Generalized Smoluchowski equation with HI

Our starting point to include HI into BD simulations is the generalization of the free-draining Smoluchowski Eq. (39) to systems of hydrodynamically interacting spherical particles. In lecture B1 by J. Dhont, the GSE including HI has been derived heuristically by means of a force balance for each colloidal particle, valid for $t \gg \tau_B$ and small density gradients only, and an exact continuity equation for the probability current. The GSE for the evolution of the configurational pdf with HI reads explicitly [5, 42]

$$\frac{\partial}{\partial t} P(\mathbf{X}, t) = \hat{\mathcal{O}}(\mathbf{X}) P(\mathbf{X}, t) , \quad (70)$$

with the Smoluchowski operator

$$\hat{\mathcal{O}}(\mathbf{X}) \equiv \nabla \cdot \mathbf{D}(\mathbf{X}) \cdot [\nabla - \beta \mathbf{F}(\mathbf{X})] = \sum_{i,j=1}^N \nabla_i \cdot \mathbf{D}_{ij}(\mathbf{X}) \cdot [\nabla_j - \beta \mathbf{F}_j(\mathbf{X})] . \quad (71)$$

Without hydrodynamic interactions, the diffusion matrix reduces to

$$\mathbf{D}_{ij}(\mathbf{X}) = D_0 \delta_{ij} \mathbf{1} , \quad (72)$$

showing that Eq. (40) for $\hat{\mathcal{O}}(\mathbf{X})$ is recovered in the free-draining limit. We recall that the applicability of the GSE is restricted to Brownian time and length scales, where both the particles

and the solvent move quasi-inertia-free. The GSE can be recast in the form ³

$$\frac{\partial}{\partial t} P(\mathbf{X}, t) = - \sum_{i=1}^N \nabla_i \cdot (\mathbf{v}_i^D(\mathbf{X}) P(\mathbf{X}, t)) + \sum_{i,j=1}^N \nabla_i \nabla_j : \mathbf{D}_{ij}(\mathbf{X}) P(\mathbf{X}, t) . \quad (73)$$

with a drift part invoking the particle drift velocities,

$$\mathbf{v}_i^D(\mathbf{X}) = \sum_{j=1}^N [\beta \mathbf{D}_{ij}(\mathbf{X}) \cdot \mathbf{F}_j(\mathbf{X}) + \nabla_j \cdot \mathbf{D}_{ij}(\mathbf{X})] , \quad (74)$$

and a diffusive part invoking the diffusivity matrix. This form of the GSE should be compared to the corresponding free-draining expression in Eq. (39). Quite interestingly, the drift velocity with HI includes an additional *hydrodynamic drift term*, $\sum_j \nabla_j \cdot \mathbf{D}_{ij}$, which is of importance when near-field HI are strong. This term accounts for changes in the local hydrodynamic particle mobility during a random step. It drives the particles in regions of higher hydrodynamic mobility, and is necessary to recover the canonical equilibrium in the course of time [43]. Physically, the hydrodynamic drift part acts similar to a radially repulsive force. In BD simulations with HI (see below), it helps thus to prevent particle overlap during a random step.

It is confirmed by inspection that $P_{eq}(\mathbf{X})$ is a stationary solution of the GSE which satisfies detailed balance. This implies that HI have no effect on static equilibrium properties, since P_{eq} is independent of the \mathbf{D}_{ij} . The positive definiteness of $\mathbf{D}(\mathbf{X})$ combined with the natural boundary conditions suffice to prove that any initially normalized and positive solution of the GSE, $P(\mathbf{X}, t)$, remains normalized and positive, and tends to P_{eq} for $t \rightarrow \infty$ [1, 10].

A Brownian Dynamics finite difference scheme for the Markov process $\mathbf{X}(t)$ with HI can be derived from the GSE, on assuming that the system has been prepared in a configuration \mathbf{X}_0 at the initial time $t_0 = 0$. After a time-step $\tau \ll \tau_a$, the configuration has changed so little that both $\mathbf{D}(\mathbf{X})$ and $\mathbf{v}^D(\mathbf{X})$ have practically remained constant. The GSE reduces then to a diffusion equation with constant coefficients,

$$\frac{\partial}{\partial \tau} W_c(\mathbf{X}, \tau | \mathbf{X}_0) = -\mathbf{v}^D(\mathbf{X}_0) \cdot \nabla W_c(\mathbf{X}, \tau | \mathbf{X}_0) + \mathbf{D}(\mathbf{X}_0) : \nabla \nabla W_c(\mathbf{X}, \tau | \mathbf{X}_0) , \quad (75)$$

where W_c is the short-time form of the conditional pdf. This equation generalizes Eq. (35) to systems with HI. The solution of Eq. (75), subject to the initial condition $W_c(\mathbf{X}, 0 | \mathbf{X}_0) = \delta(\mathbf{X} - \mathbf{X}_0)$, is given by

$$W_c(\mathbf{X}, \tau | \mathbf{X}_0) = \{4\pi\tau\}^{-3N/2} \frac{1}{(\det \mathbf{D}(\mathbf{X}_0))^{1/2}} \cdot \exp\left\{-\frac{1}{4\tau} [\mathbf{X} - \mathbf{X}_0 - \tau \mathbf{v}^D(\mathbf{X}_0)]^T \cdot \mathbf{D}^{-1}(\mathbf{X}_0) \cdot [\mathbf{X} - \mathbf{X}_0 - \tau \mathbf{v}^D(\mathbf{X}_0)]\right\} . \quad (76)$$

as can be checked by substitution (cf. Eq. (34)). A direct proof is obtained through the change of variables from \mathbf{X} to \mathbf{Y} ,

$$\mathbf{X} - \tau \mathbf{v}^D(\mathbf{X}_0) = \mathbf{d}(\mathbf{X}_0) \cdot \mathbf{Y} \implies \frac{\partial}{\partial \mathbf{X}} = \mathbf{d}^{-1}(\mathbf{X}_0) \cdot \frac{\partial}{\partial \mathbf{Y}} , \quad (77)$$

³Here, $\nabla_i \nabla_j : \mathbf{D}_{ij} P = \nabla_i \cdot [\nabla_j \cdot (\mathbf{D}_{ij} P)]$.

which transforms Eq. (75) into a standard Gaussian form which can be easily solved. Here, \mathbf{d} is the square-root matrix of the positive definite matrix \mathbf{D} , defined by $\mathbf{D} = \mathbf{d} \cdot \mathbf{d}^T$. We note from Eq. (76) that, in common with the free-draining approximation, $\mathbf{X}(\tau)$ is Gaussian for short time displacements. With HI, however, the particle positions are coupled even at small τ . Moreover, one can show that non-Gaussian corrections to W_c start to develop earlier with than without HI when τ is increased (see [33] for details).

4.3 Finite difference algorithms including HI

On noticing that $P_c(\mathbf{X}, \tau | \mathbf{X}_0) = W_c(\mathbf{X}, \tau | \mathbf{X}_0) + o(\tau)$, and that W_c describes a Gaussian process, the conditional moments defined in Eq. (44) are straightforwardly calculated, using Eq. (76), as

$$\langle \Delta \mathbf{X}_i(\tau) \rangle_0 = \mathbf{v}_i^D(\mathbf{X}_0) \tau + o(\tau) \quad (78)$$

$$\langle \Delta \mathbf{X}_i(\tau) \Delta \mathbf{X}_j(\tau) \rangle_0 = 2 \mathbf{D}_{ij}(\mathbf{X}_0) \tau + o(\tau), \quad (79)$$

with all higher-order moments being small of $o(\tau)$. The hydrodynamic coupling of the short-time displacements between different particles and the symmetry of the diffusivity matrix is made explicit in the covariance matrix in Eq. (79), which expresses a fluctuation-dissipation relation.

Knowing Eq. (76) and its moment relations, we are in the position to formulate the finite-difference equation including HI,

$$\mathbf{r}_i(t_0 + \tau) = \mathbf{r}_i(t_0) + \mathbf{v}_i^D(\mathbf{X}_0) \tau + \sqrt{2\tau} \mathbf{d}(\mathbf{X}_0) \cdot \mathbf{n} + o(\tau), \quad (80)$$

which is stochastically equivalent to Eq. (70) in the limit $\tau \rightarrow 0$. Eq. (80) is the extension of Ermak's first-order forward integration scheme to systems where HI is included. It is commonly referred to as the *Ermak-McCammon scheme* [7]. Like in the free-draining limit, \mathbf{n} is a Gaussian random vector of independently distributed components of mean zero and variance one. These components are most conveniently calculated, to first order in τ , using Eq. (50).

To obtain the random displacement part in Eq. (80) for given initial configuration \mathbf{X}_0 requires, in principle, to determine the positive definite $3N \times 3N$ square-root matrix $\mathbf{d}(\mathbf{X}_0)$. The matrix \mathbf{d} is not uniquely determined by its defining equation

$$\mathbf{D}(\mathbf{X}_0) = \mathbf{d}(\mathbf{X}_0) \cdot \mathbf{d}^T(\mathbf{X}_0). \quad (81)$$

One may additionally demand that \mathbf{d} is a symmetric matrix. This requires for its determination to compute the eigenvalues of \mathbf{D} , which are all necessarily positive. Alternatively and preferentially, \mathbf{d} may be chosen to be a lower triangular matrix. Then a lower-upper decomposition of the diffusivity matrix is required which can be done using the standard Cholesky decomposition algorithm [11, 44, 45]. Both alternatives to determine $\mathbf{d}(\mathbf{X}_0)$ amount to $O(N^3)$ operations at each time-step. This is the reason why calculations of \mathbf{d} form the bottleneck of BD simulations including HI, leading to severe restrictions in the number of simulated particles. In fact since only the product $\mathbf{d} \cdot \mathbf{n}$ is needed instead of \mathbf{d} alone, actual calculations of the random displacement can be speeded up to roughly an $O(N^{2.25})$ operation, by means of a Chebyshev polynomial approximation proposed originally by Fixman [46] (see also [38]).

A disadvantage of the one-step Ermak-McCammon scheme is that it requires, at each time-step, the computationally expensive calculation of $\nabla_0 \cdot \mathbf{D}(\mathbf{X}_0)$, when the system is so dense that the

Rotne-Prager approximation is not sufficient. It is possible to calculate the hydrodynamic drift term analytically by means of a multipole expansion method [47], which is more accurate and less expensive in terms of computer time and memory than a 'brute-force' numerical differentiation. Alternatively, one may use an elegant updating algorithm developed by Fixman. This algorithm involves a midpoint evaluation, which avoids the explicit calculation of the divergence of \mathbf{D} , at the less severe expense of a two-step calculation for each time-step τ . Using the abbreviation $\mathbf{R}^s(\tau) \equiv \sqrt{2\tau} \mathbf{n}$, Fixman's algorithm [46] may be formulated as follows (see also [48, 49]):

- (i) For a time-step $\tau \ll \tau_a$, calculate first the midpoint configuration \mathbf{X}^* , using

$$\mathbf{X}^* = \mathbf{X}_0 + \frac{1}{2} \mathbf{D}(\mathbf{X}_0) \cdot \left[\beta \mathbf{F}(\mathbf{X}_0) \tau + (\mathbf{d}^T(\mathbf{X}_0))^{-1} \cdot \mathbf{R}^s(\tau) \right]. \quad (82)$$

Note that only one half of the force drift part and random displacement part is involved, and that the hydrodynamic drift part is suppressed.

- (ii) In a second step, calculate the actual configuration after the time-step τ according to

$$\mathbf{X} = \mathbf{X}_0 + \mathbf{D}(\mathbf{X}^*) \cdot \left[\beta \mathbf{F}(\mathbf{X}^*) \tau + (\mathbf{d}^T(\mathbf{X}_0))^{-1} \cdot \mathbf{R}^s(\tau) \right]. \quad (83)$$

The random *force*, $(\mathbf{d}^T(\mathbf{X}_0))^{-1} \cdot \mathbf{R}^s(\tau)$, has been kept constant over the full time-step, whereas the small change in configuration is accounted for in the diffusivity matrix. To see that Fixman's midpoint BD algorithm is equivalent to the Ermak-McCammon scheme to first order in τ , Taylor-expand $\mathbf{F}(\mathbf{X}^*)$ and $\mathbf{D}(\mathbf{X}^*)$ to leading order in $(\mathbf{X}^* - \mathbf{X}_0)$, using (i), and convince yourself that the moment relations in Eqs. (78) and (79) are recovered.

A remarkable consequence of accounting for near-field HI and lubrication in BD simulations is that since the *relative* motion of two very nearby particles is almost completely suppressed due to the stick boundary conditions, no non-hydrodynamic excluded volume forces are needed to satisfy the zero relative radial flux boundary conditions. It is therefore possible to simulate hydrodynamically interacting hard spheres without excluded volume forces [50]. The probability current in the continuity equation form, Eq. (42), of the GSE is generalized with HI to

$$\begin{aligned} \mathbf{j}_i(\mathbf{X}, t) &= - \sum_{l=1}^N \mathbf{D}_{il}(\mathbf{X}) \cdot [\nabla_l - \beta \mathbf{F}_l(\mathbf{X})] P(\mathbf{X}, t) \\ &= \mathbf{v}_i^D(\mathbf{X}) P(\mathbf{X}, t) - \sum_{l=1}^N \nabla_l \cdot \mathbf{D}_{il}(\mathbf{X}) P(\mathbf{X}, t). \end{aligned} \quad (84)$$

Using this expression, the zero-relative-flux boundary condition for two isolated spheres 1 and 2 in contact is

$$\hat{\mathbf{r}}_{12} \cdot \mathbf{D}_{12}^{rel}(\mathbf{r}_{12}) \cdot [\nabla_{12} - \beta \mathbf{F}_{12}] P(\mathbf{r}_{12}, t)|_{r_{12}=\sigma^+} = 0. \quad (85)$$

For hard spheres, $\mathbf{F}_{12} \sim \delta(r_{12} - \sigma) \hat{\mathbf{r}}_{12}$ is the singular force exerted on sphere 1 by sphere 2, and $\mathbf{D}^{rel} = \mathbf{D}_{11} + \mathbf{D}_{22} - \mathbf{D}_{12} - \mathbf{D}_{21}$ is the relative diffusivity tensor. The hard-sphere force drops out of the zero-flux condition since $\hat{\mathbf{r}}_{12} \cdot \mathbf{D}_{12}^{rel}(\mathbf{r}_{12}) \sim (r_{12} - \sigma)$, for $r_{12} \rightarrow \sigma$, and $(r - \sigma)\delta(r - \sigma) = 0$. Consequently, the hard-sphere potential plays no dynamical role in BD simulations of hard spheres with a full account of near-field HI [51].

Note here that the Brownian motion of colloidal hard spheres keeps them apart and well dispersed. Particles can get linked together by strong lubrication forces, eventually forming non-compact aggregates, only when the suspension is subject to a very strong shearing motion which totally dominates the Brownian random excursions described by the random displacement term in the BD finite difference equation [50, 52]. The motion of hydrodynamically interacting, and typically quite large mesoparticles [53], in a regime where Brownian random displacements can be *neglected* is referred to as *Stokesian Dynamics*, since the HI are described by the Stokes equation. Contrary to Brownian Dynamics, where the particle motion is kept alive by the thermal bombardment of solvent molecules, Stokesian Dynamics requires an *external* forcing, for example in the form of an imposed shear flow caused by moving system boundaries, or strong sedimentation forces, to keep the particles moving (see, e.g., [54]). Be alerted here against a possible source of confusion: in part of the literature, and different from the present usage, Stokesian Dynamics is referred to as a special form of Brownian Dynamics including random motion, where many-body HI and lubrication effects have been accounted for. To avoid confusion, sometimes the more explicit notion 'Stokesian Dynamics of Brownian suspensions' is used for a simulation scheme which accounts for Brownian random displacements in addition to near-field HI (see, e.g., [51]).

In BD studies of unbound suspensions, additional problems arise from the long-range nature of HI, and from using periodic boundary conditions. Obviously, these problems are present even when near-field HI is negligible or simply disregarded. A simple summation of the far-field hydrodynamic interactions results in badly divergent expressions. However, these convergence problems can be overcome using a regularizing hydrodynamic Ewald summation technique [55], adapted to an infinite periodic system [56–58]. The hydrodynamic regularization procedure is an additional expensive ingredient in a BD simulation study with HI.

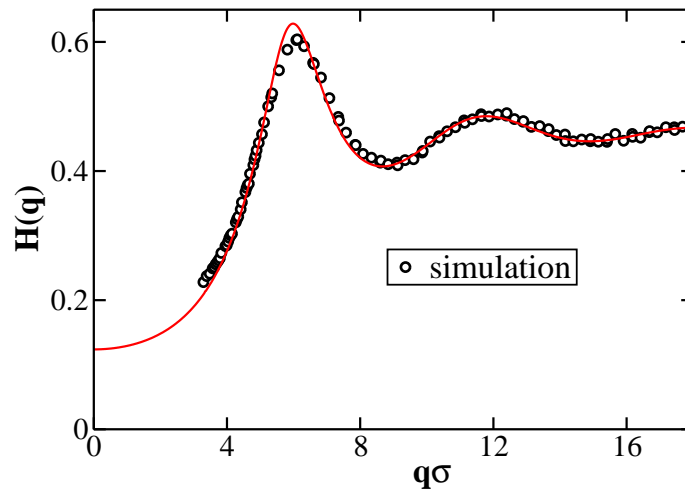


Fig. 9: BD simulation result with many-body HI for the $H(q)$ of charged globular proteins at volume fraction $\phi = 0.33$. The simulation has been performed using $N = 860$ particles (from [16]).

An important measure of the strength of HI with regard to particle diffusion is given by the hydrodynamic function, $H(q)$, defined and computable as [3]

$$H(q) = \frac{1}{ND_0} \left\langle \sum_{l,j=1}^N \hat{\mathbf{q}} \cdot \mathbf{D}_{lj}(\mathbf{X}) \cdot \hat{\mathbf{q}} \exp\{i\mathbf{q} \cdot [\mathbf{r}_l - \mathbf{r}_j]\} \right\rangle_M, \quad (86)$$

with $\hat{\mathbf{q}} = \mathbf{q}/q$. The function $H(q)$ is non-negative and contains, through the diffusivity tensors \mathbf{D}_{ij} , the influence of HI on the short-time collective diffusion of particles caused by local density gradients. This explains why $H(q)$ is referred to as the *hydrodynamic function*. Recall here that the colloidal short-time regime is defined by $\tau_B \ll t \ll \tau_a$. Experimentally, $H(q)$ is determined as a function of the wavenumber q through a combination of static and dynamic scattering experiments [3]. Without HI, $H(q) = 1$ so that any variation in $H(q)$ is a hallmark of HI. The function $H(q)$ has a direct physical meaning as the (reduced) mean particle sedimentation velocity for a suspension subject to a weak periodic force field, collinear with the wavevector \mathbf{q} and oscillating like $\cos(\mathbf{q} \cdot \mathbf{r})$. The long-wavelength limit of $H(q)$ is thus equal to the (short-time) reduced sedimentation velocity of slightly non-buoyant particles forming a homogeneous suspension.

Fig. 9 includes a BD simulation result for the hydrodynamic function of charged spherical proteins. The radial distribution function of this system is shown in Fig. 5. The most important HI contribution to $H(q)$ arises from the many-body near-field part $\Delta\mathbf{D}_{ij}$ since, as noticed from Fig. 5, $g(r)$ is non-zero at contact. The near-field part is responsible for a value of the peak height of $H(q)$ *smaller* than one. In dilute charge-stabilized suspensions, where Rotne-Prager far-field HI prevails, $H(q)$ is characterized instead by a peak height *larger* than one [3]. Fig. 9 has been obtained using a recently developed accelerated BD code where HI is fully accounted for. This code allows to compute short-time dynamic properties using a large number of particles (see [59] and the discussion in the final part of section 5).

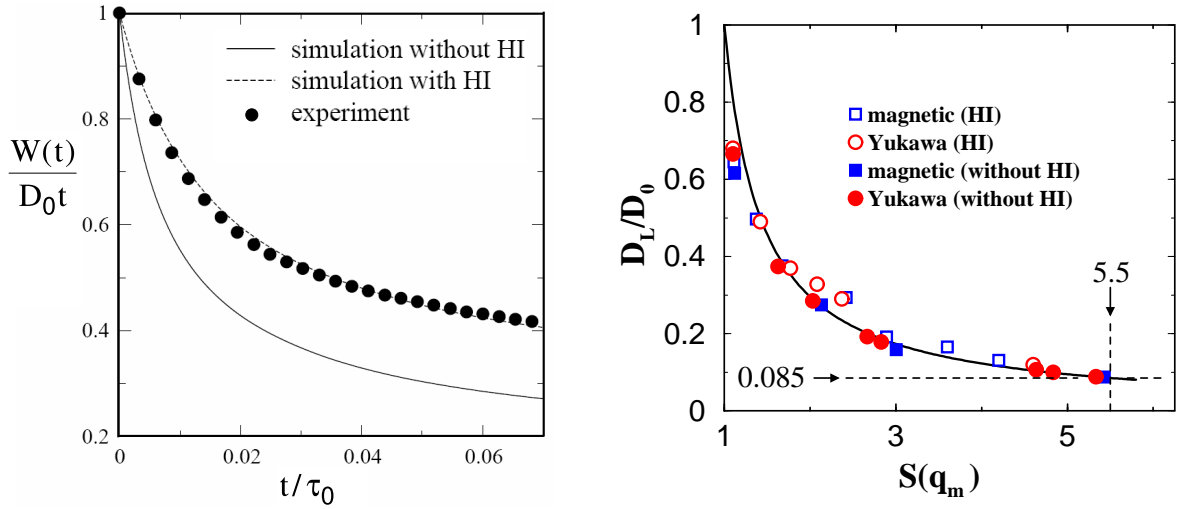


Fig. 10: Left: BD simulation of the reduced mean-square displacement for magnetic spheres of areal number density $\rho = 3.24 \times 10^{-3} \mu\text{m}^{-2}$, moving along an air-water interface (from [60]). Right: Long-time self-diffusion coefficient, D_L , versus maximum height, $S(q_m)$, of the static structure factor of quasi-two-dimensional systems (from [61]).

Unlike the system of Fig. 9, semi-dilute suspensions with strong and long-range particle repulsions are dominated in their dynamics by the pairwise-additive far-field part of the HI. Examples of such systems, which have been extensively studied in the past, are suspensions of magnetic or charged colloidal spheres confined to two-dimensional translational motion. A well-studied quasi-two-dimensional system of this sort consists of super-paramagnetic colloidal spheres confined by gravity to motion along a planar water-air interface [60]. The spheres in this system repel each other by forces described *very* accurately by the dipolar pair potential $u(r) = \mu_0 M^2 / (4\pi r^3)$, where M is the magnetic moment of a sphere induced by an external

magnetic field directed perpendicular to the interface, and μ_0 is the vacuum magnetic constant. An experimentally determined MSD for such a system is shown in the left part of Fig. 10, in comparison with BD simulation results with far-field HI included and without HI. Time is measured here in units of $\tau_0 = 1/(\rho D_0)$, which is the time needed for a particle to diffuse across an inter-particle distance, $\rho^{-1/2}$, in the absence of any interactions. Contrary to the near-field part of HI, which slows down self-diffusion, far-field HI causes a significant increase in $W(t)$. The hydrodynamic enhancement of self-diffusion caused by far-field HI is a generic feature observed in all (semi-dilute) quasi-two-dimensional *and* three-dimensional suspensions with long-range inter-particle repulsions [3]. As an aside, we note that the HI between spheres moving along a liquid-gas interface differs from that in an unbound fluid. A derivation and discussion of the quasi-two-dimensional analog of the three-dimensional Rotne-Prager diffusivity tensor for particles at a liquid-gas interface can be found in [62].

Quasi-two-dimensional suspensions of particles characterized by a single static length scale show an interesting form of dynamic scaling depicted in the right part of Fig. 10, where BD simulated results for the long-time self-diffusion coefficient, D_L , with and without far-field HI are plotted as function of the peak height, $S(q_m)$, of the static structure factor. Results are shown both for super-paramagnetic and charged spheres, whereby the latter have been assumed to interact by a Yukawa-like screened Coulomb potential similar to the one in Eq. (54). As can be seen, D_L is determined essentially by $S(q_m)$ alone, independent from the details of the pair interaction. At a fluid-solid transition point, one observes that $D_L/D_0 \approx 0.085$ which corresponds to a structure factor peak height of $S(q_m) \approx 5.5$. These values are in quantitative accord with empirically found static and dynamic criteria for the onset of freezing in two-dimensional systems (for details see [61, 63]).

5 Summary and Outlook

Brownian Dynamics simulations are a versatile and frequently applied tool to study diffusion, rheology and microstructural properties of dispersions of mesoscaled particles, like colloids and polymers, on time and length scales where configurational changes take place.

In this lecture, only systems of monodisperse spherical particles have been considered and, as an additional restriction, only their translational motion. The Ermak-McCammon scheme of hydrodynamically interacting spheres is easily extended to include the translational-rotational motion of the particles [64]. Moreover, mixtures of colloidal spheres have been treated in BD simulations both with [65] and without HI [66].

The effect of an ambient shear flow [40, 44] can be implemented into the simulation scheme, by adding an affine displacement to the rhs of Eq. (80) caused by the shearing motion, and by adjusting the periodic boundary conditions appropriately [11, 44]. The stationary pdf for systems under steady shear is not given any more by the canonical distribution function, since the average local environment of a particle is deformed away from spherical symmetry. BD simulations of flexible linear aggregates formed by spheres which are interacting by far-field HI only, are common practice nowadays. Such bead-spring-type models are used to explore generic properties of dilute solutions of homopolymers and DNA [39], and short-chain polyelectrolytes [67].

The HI between non-spherical rigid particles are very complicated, and not well understood to date even in the most simple case of uniaxial rods. For this reason, the dynamics in colloidal suspensions of rod-like neutral [68, 69] and charged [70] particles has been investigated almost

exclusively in free-draining BD simulations.

In free-draining simulations, up to a few thousand particles can be simulated, which greatly helps to improve the statistics of computed properties. BD simulations with HI require a substantially larger numerical effort, so that the number of particles in three-dimensional simulations is limited to at most a few hundred. Recently, a new implementation of the BD simulation method with a full account of HI has been developed, in which the computational cost is strongly reduced to an $O(N \ln N)$ algorithm [59]. This acceleration of the BD algorithm has been achieved using a grid-based scheme for the far-field HI part along with an Ewald summation technique. The new scheme allows simulations of the order of 1000 particles. It has been applied recently to study the dynamics in rather dense solutions of charged globular proteins [16].

To describe the rheology of very dense suspensions of closely spaced hard spheres at and above the volume fraction $\phi = 0.494$ where the suspension starts to freeze into a solid, a so-called lubrication approximation has been proposed, in which the diffusivity matrix is calculated using the lubrication forces alone. Since the numerically expensive long-range part of the HI has been ignored in this approximation, it is possible to simulate a few thousand particles [49].

References

- [1] N.G. van Kampen, *Stochastic Processes in Physics and Chemistry* (North-Holland, Amsterdam, 1985)
- [2] C.W. Gardiner, *Handbook of Stochastic Methods* (2nd Edition, Springer, Berlin, 1990)
- [3] G. Nägele, J.K.G. Dhont and G. Meier in "Diffusion in Condensed Matter", Eds. P. Heitjans and J. Kärger, Springer-Verlag, Berlin (2005)
- [4] E.J. Hinch, *J. Fluid. Mech.* **72**, 499 (1975)
- [5] G. Nägele, *Phys. Rep.* **272**, 215 (1996)
- [6] G.N. Paul and P.N. Pusey, *J. Phys. A* **14**, 3301 (1981)
- [7] D.J. Ermak and J.A. McCammon, *J. Chem. Phys.* **69**, 1352 (1978)
- [8] D.J. Ermak, *J. Chem. Phys.* **62**, 4189 (1975)
- [9] J. Honerkamp, *Stochastische Dynamische Systeme* (VCH, Weinheim, 1990)
- [10] H. Risken, *The Fokker-Planck Equation* (Springer, Berlin, 1996)
- [11] M.P. Allen and D.J. Tildesley, *Computer Simulation of Liquids* (Oxford Science Publications, Clarendon Press, Oxford, 1987)
- [12] C. Holm in "Computational Soft Matter: From Synthetic Polymers to Proteins", pp. 195-236, Eds. N. Attig et al., John von Neumann Institute for Computing (NIC series), Vol. 23, Research Centre Jülich (2004)
- [13] G.E.P. Box and M.E. Müller, *Ann. math. Stat.* **29**, 610 (1958)
- [14] A. Greiner, W. Strittmaier and J. Honerkamp, *J. Stat. Phys.* **51**, 95 (1987)
- [15] B. Dünweg and W. Paul, *Int. J. Mod. Phys. C* **2**, 817 (1991)
- [16] J. Gapinski, A. Wilk, A. Patkowski, A.J. Banchio, R. Pecora and G. Nägele, *J. Chem. Phys.* **123**, 054708 (2005)
- [17] B. Cichocki, *Z. Phys. B* **66**, 537 (1987)
- [18] D.M. Heyes and A.C. Branka, *Phys. Rev. E* **50**, 2377 (1994)
- [19] D.M. Heyes and P.J. Mitchell, *J. Chem. Soc. Faraday Trans.* **90**, 1931 (1994)
- [20] W. Schaertl and H. Sillescu, *J. Stat. Phys.* **74**, 687 (1994); *ibid.* **79**, 299 (1995)
- [21] D.R. Foss and J.F. Brady, *J. Rheol.* **44**, 629 (2000)
- [22] P. Strating, *Phys. Rev. E* **59**, 2175 (1999)
- [23] Y. Terada and M. Tokuyama, *J. Korean Phys. Soc.* **38**, 512 (2001)

- [24] T.M.A.O.M. Barenbrug, E.A.J.F. Peters and J.D. Schieber, *J. Chem. Phys.* **117**, 9202 (2002)
- [25] P.J. Rossky, J.D. Doll and H.L. Friedman, *J. Chem. Phys.* **69**, 4628 (1978)
- [26] D. Ceperley, M.H. Kalos and J.L. Lebowitz, *Macromolecules* **14**, 1472 (1981)
- [27] B. Cichocki and K. Hinsén, *Physica A* **166**, 473 (1990)
- [28] D.M. Heyes and A.C. Branka, *Mol. Phys.* **94**, 447 (1998)
- [29] D.M. Heyes and A.C. Branka, *Mol. Phys.* **98**, 1949 (2000)
- [30] M. Jardat, O. Bernard, P. Turq and G. Kneller, *J. Chem. Phys.* **110**, 7993 (1999)
- [31] B. Cichocki and K. Hinsén, *Physica A* **187**, 133 (1992)
- [32] B. Cichocki and B.U. Felderhof, *Physica A* **204**, 152 (1994)
- [33] R.J.A. Tough, P.N. Pusey, H.N. Lekkerkerker and C. van den Broeck, *Molec. Phys.* **59**, 595 (1986)
- [34] J.K.G. Dhont, *An Introduction to Dynamics of Colloids* (Elsevier, Amsterdam, 1996)
- [35] S. Kim and S.J. Karrila, *Microhydrodynamics: Principles and Selected Applications* (Butterworth-Heinemann, 1991)
- [36] J.C. van der Werff, C.G. de Kruiff, C. Blom and J. Mellema, *Phys. Rev. A* **39**, 795 (1989)
- [37] J. Rotne and S. Prager, *J. Chem. Phys.* **50**, 4831 (1969)
- [38] R.M. Jendrejack, M.D. Graham and J.J. de Pablo, *J. Chem. Phys.* **113**, 2894 (2000)
- [39] C.C. Hsieh, L. Li and R.G. Larson, *J. Non-Newtonian Fluid Mech.* **113**, 147 (2003)
- [40] H.C. Öttinger, *Stochastic Processes in Polymeric Fluids* (Springer, Berlin, 1996)
- [41] W. Zylka and H.C. Öttinger, *J. Chem. Phys.* **90**, 474 (1989)
- [42] G. Nägele, *The Physics of Colloidal Soft Matter*, Lecture Notes 14, Polish Academy of Sciences Publishing, Warsaw (2004)
- [43] M. Doi and S.F. Edwards, *The Theory of Polymer Dynamics* (Oxford Science Publications, Clarendon Press, Oxford, 1986)
- [44] A. Satoh, *Introduction to Molecular-Microsimulation of Colloidal Dispersions* (Elsevier, Amsterdam, 2003)
- [45] W.H. Press, S.A. Teukolsky, W.V. Vetterling and B.P. Flannery, *Fortran Numerical Recipes* (Cambridge University Press, Cambridge, 1996)
- [46] M. Fixman, *Macromolecules* **19**, 1195; 1204 (1986)
- [47] E. Wajnryb, P. Szymczak and B. Cichocki, *Physica A* **335**, 339 (2004)

- [48] P.S. Grassia, E.J. Hinch and L.C. Nitsche, *J. Fluid Mech.* **282**, 373 (1995)
- [49] R.C. Ball and J.R. Melrose, *Physica A* **247**, 444 (1997)
- [50] D.R. Foss and J.F. Brady, *J. Fluid Mech.* **407**, 167 (2000)
- [51] T.N. Phung, J.F. Brady and G. Bossis, *J. Fluid Mech.* **313**, 181 (1996)
- [52] R.C. Ball and J.R. Melrose, *Adv. Colloid Interface Sci.* **59**, 19 (1995)
- [53] A.J.C. Ladd in "Computer Simulations of Surfaces and Interfaces", Eds. B. Dünweg et al., pp. 175-188, NATO science series II: Mathematics, Physics and Chemistry - Vol. 114, Kluwer, Dordrecht (2003)
- [54] K. Hinsén and R. Kneller, *J. Mol. Model.* **2**, 227 (1996)
- [55] C.W.J. Beenakker, *J. Chem. Phys.* **85**, 1581 (1986)
- [56] E.R. Smith, I.K. Snook and W. van Megen, *Physica A* **143**, 441 (1987)
- [57] J.F. Brady and G. Bossis, *J. Fluid Mech.* **20**, 111 (1988)
- [58] B.U. Felderhof, *Physica A* **159**, 1 (1989)
- [59] A.J. Banchio and J.F. Brady, *J. Chem. Phys.* **118**, 10323 (2003)
- [60] B. Rinn, K. Zahn, P. Maass and G. Maret, *Europhys. Lett.* **46**, 537 (1999)
- [61] G. Nägele, M. Kollmann, R. Pesché and A.J. Banchio, *Molec. Phys.* **100**, 2921 (2002)
- [62] B. Cichocki, M.L. Ekiel-Jezewska, G. Nägele and E. Wajnryb, *Europhys. Lett.* **67**, 383 (2004)
- [63] H. Löwen, *Phys. Rev. E* **53**, R29 (1996)
- [64] E. Dickinson, *J. Chem. Soc., Faraday Trans. 2* **81**, 591 (1985)
- [65] M. Kollmann, R. Hund, B. Rinn, G. Nägele, K. Zahn, H. König, G. Maret, R. Klein und J.K.G. Dhont, *Europhys. Lett.* **58**, 919 (2002)
- [66] S. Sanyal and A.J. Sood, *Phys. Rev. E* **57**, 908 (1998)
- [67] T. Zhou and S.B. Chen, *J. Chem. Phys.* **124**, 034904 (2006)
- [68] H. Löwen, *Phys. Rev. E* **50**, 1232 (1994)
- [69] Y.-G. Tao, W.K. den Otter, J.T. Padding, J.K.G. Dhont and W.J. Briels, *J. Chem. Phys.* **122**, 244903 (2005)
- [70] Th. Kirchhoff, H. Löwen and R. Klein, *Phys. Rev. E* **53**, 5011 (1996)